Validation of the SAFER Human Body Model Kinematics in Far-Side Impacts

Validation of the SAFER Human Body Model Kinematics in Far-Side Impacts

Bengt Pipkorn, Jonas Östh, Erik Brynskog, Emma Larsson, Liselotte Rydqvist, Johan Iraeus, Daniel Perez-Rapela, Lotta Jakobsson

Abstract Human Body Models are essential for real-world occupant protection assessment. With the overall purpose to create a robust human body model which is biofidelic in a variety of crash situations, this study aims to evaluate the biofidelity of the SAFER human body model in far-side impacts. The pelvis, torso and the upper and lower extremities of the SAFER human body model were updated. In addition, the shoulder area was updated for improved shoulder belt interaction in far-side impacts. The model was validated using kinematic corridors based on published human subject test data from two far-side impact set-ups, one simplified and one vehicle-based. The simplified far-side set-up included six configurations with different parameter settings, and the vehicle-based included two configurations: with and without far-side airbag, respectively.

The updated SAFER HBM was robust and in general the model predicted the published human subject responses (kinematic CORA score > 0.65) for all configurations in both test set-ups. An exception was a 90 degree far-side impact with the D-ring in the forward position, in the simplified set-up. Here the model could not predict the shoulder belt retention, resulting in a low CORA score. Based on the overall results, the model is considered valid to be used for assessment of far-side impact countermeasures.

Keywords Euro NCAP, Far-side, SAFER HBM, Validation, Virtual Testing.

I. INTRODUCTION

Real-world occupant protection requires methods and tools capable of predicting the large variety of crashes occurring in real traffic. Thanks to their anatomically based design, Finite Element Human Body Models (FE-HBMs) have the potential to predict human kinematics and injury risks in omnidirectional crash loading. To ensure biofidelic performance, the model needs to be validated using physical tests reflecting the variety of occupant loading seen in real-world traffic situations.

Reference [1] analysed Australian and US data and reported that for seriously injured (AIS3+) occupants using 3-point seatbelts, approximately 20% of the occupants in side impacts were seated on the non-struck side (so called far-side impacts). The head and thorax are the most frequently injured body regions for occupants in far-side impacts [1-4]. Belt slipping off the shoulder has been attributed as a contributing factor to head injuries [5], resulting in head impacts against the intruding struck-side interior [6]. Early studies on far-side impact countermeasures include side support airbags [6-7] and altered three-point belt geometry [6].

Recently, far-side impacts have been addressed as a test configuration in consumer information testing, for instance through a physical crash test in the European New Car Assessment Programme (Euro NCAP) 2020 protocol [8]. When announcing ambitions for virtual testing, far-side impact was selected as the pilot test set-up by Euro NCAP and was included in the roadmap for future protocols [9]. The proposal includes virtual sled evaluation with numerical models of the WorldSID anthropomorphic test device (ATD) and at a later stage using HBMs. However, for HBMs, unlike for ATDs, there is yet no standardisation of models. Therefore, more work is needed to develop methods which can prove that an HBM is valid and applicable to be used for virtual test protocols. The biofidelity of the model should be proven by validating the model by comparison to Post-Mortem Human Subjects (PMHSs) tests carried out in relevant test configurations.

B. Pipkorn (bengt.pipkorn@autoliv.com; +46 (0)322 626341) is Director of Simulation and Active Structures and L. Rydqvist is a Safety Analysis CAE Engineer at Autoliv, Vårgårda, Sweden. J. Östh, PhD, is a Safety Analysis CAE Engineer and L. Jakobsson is Senior Technical Leader in Injury Prevention at the Volvo Cars Safety Centre, Gothenburg, Sweden. E. Brynskog and E. Larsson are PhD students, J. Iraeus a Senior Researcher, B. Pipkorn and L. Jakobsson Adjunct Professors, and J. Östh an Adjunct Associate Professor at Chalmers University of Technology, Gothenburg, Sweden. Daniel Perez-Rapela is a Postdoctoral Research Associate at the University of Virginia Center for Applied Biomechanics, Charlottesville, VA, USA

Several studies have investigated kinematic and kinetic responses of PMHS and ATDs in far-side impacts. An early study included five current side impact test dummies and one PMHS, using a combination of a whole vehicle test and a similar full-scale validated sled test set-up [10]. Using a simplified far-side impact buck, [11] performed match-paired tests with PMHSs, WorldSID and THOR, respectively, including generic countermeasures such as shoulder or thorax plates and an inboard shoulder belt. Both ATDs provided good measures of head excursion compared to the PMHS across most configurations, although having difficulties in measuring appropriate chest deformations. Another simplified test environment was developed by [12], and used for an extensive parametric study of the influence of restraint conditions on responses of PMHSs. Restrained by 3-point-seatbelts, seven PMHS were subjected to repeated tests varying the D-ring position, arm position, pelvis restraint, pre-tensioning and impact severity, in total 36 tests. The tests provided insights into the complexity and challenges of occupant restraint kinematics in far-side lateral and oblique impacts, in addition to valuable data for validation of occupant models. Reference [13] followed-up with physical tests with WorldSID and compared to the PMHS tests. The results showed discrepancies in shoulder-belt engagement, head and torso kinematics and sensitivity to initial conditions. A computational model of the simplified test set-up in [12] was created by [14] and used to assess the biofidelity of a modified detailed Global Human Body Models Consortium (GHBMC) model. The updated model, including mainly thoracic and lumbar spine modifications, was shown sensitive to the varied parameters [12], in-line with the trends observed in the PMHS tests [12]. Similar studies were also performed with a modified Total Human Model for Safety (THUMS) [15] and the simplified GHMBC [16]. For the modified THUMS it was found that the model could be used to predict head excursion and the risk of rib fracture [15]. The simplified GHBMC showed good agreement with PMHS kinematics [16].

With the aim of developing injury criteria limits, [17] executed six paired PMHS / WorldSID tests following the Euro NCAP test protocol proposal, at two severities (ΔV of 8 m/s and 11 m/s). The peak head excursion predicted by the WorldSID were found reasonably similar. However, the ATD repeatability was found to be poor, influenced by neck damage and lap belt forces. A neck injury risk criterion applicable to both the upper and lower neck was derived, also taking the results from [11-12] into account.

Using a vehicle-like environment, [18] executed five PMHS and four WorldSID tests using a vehicle interior fixture, based on a mid-size sedan. The fixture included the vehicle's driver and passenger seat, a centre console and seatbelts. The seatbelt included a retractor with a pretensioner and a 2 kN load-limiter. The vehicle fixture was exposed to a crash pulse matching the Euro NCAP far-side assessment protocol. The WorldSID captured the PMHS's lateral chest deflection and exhibited PMHS-like shoulder belt force until it lost contact with the shoulder belt, when slipping out, presumably due to its stiffer upper body. Using the same test set-up, but adding a far-side airbag, [19] performed tests with three PMHSs and one WorldSID. In addition to comparing the WorldSID and PMHS responses in a different occupant boundary condition, the study aimed at investigating the far-side airbag effectiveness, by comparing the results from the two studies [18-19]. It was seen that while the far-side airbag concept not only reduced maximum lateral head excursion by 14.6%, it also reduced lateral excursion variance for the PMHSs. It was concluded that the reduction in lateral excursion in combination with the fact that the airbag remained pressurised after the event, indicated that the restraint also was able to prevent occupant-to-occupant interaction [19].

The vehicle-like environment in [18-19] provides a good complement to the simplified far-side impact test set-up [12] as a platform for validation of HBMs. Specifically, it provides more similarities to how it will be used in countermeasure development and evaluation. Hence, with the overall purpose of creating a robust HBM which is biofidelic for a variety of real-world crash situations, the aims of this study are to implement changes to improve the SAFER HBM's overall biofidelity and to evaluate its biofidelity in far-side impact, using published data. The improvements include several body regions of the SAFER HBM. Two different far-side impact set-ups with several configurations serve as the platform for its validation.

II. METHODS

The SAFER HBM was updated in the pelvis, torso, upper extremity, and lower extremity areas and evaluated for far-side impact predictions by validation to previously published PMHS tests [12][18-19], in total eight different configurations. First, the biofidelity of the updated SAFER HBM was evaluated in six configurations using a simplified rigid planar seat far-side set-up [12] with well-defined boundary conditions. Second, the validation was extended using a vehicle-based test set-up [18-19], including a production car seat and centre console. The

latter set-up was evaluated for two different boundary conditions: without and with a far-side airbag. All simulations were conducted using LS-DYNA (LST, Livermore, CA, USA) MPP R9.3.1 Single Precision. The SAFER HBM, a 50th percentile male (175 cm, 77 kg [20]) model, originally based on the THUMS v3, but as of the v10 update described in this study, most parts have been updated or replaced. Previous model updates include the replacement of the head with the KTH Royal Institute of Technology (KTH) head model [21], a rib cage with statistically based 50th percentile male shape [20] and updated cervical and lumbar spine [22]. The model has an active muscle package utilising feedback control to model human postural control [23-24] in the pre-crash phase.

HBM Updates

A new pelvis model, representing that of a 50th percentile male (50 years old, 175 cm and 77 kg) was defined using Sparse Principal Component Analysis on 57 male Computed Tomography (CT) scans. The two innominate bones and sacrum were modelled as a sandwich structure with hexahedral elements for the trabecular core covered with quadrilateral elements representing the cortical surface. The pubic symphysis was modelled as a composite of hexahedral and quadrilateral elements, and assigned viscohyperelastic materials based on [25]. The sacroiliac (SI) joint was modelled as a combination of hexahedral elements, representing the interosseous ligaments, and hexahedral elements with a sliding contact, for the articulating surfaces, with material data assumed to be similar to that of the pubic symphysis disc. Additional ligaments of the pelvis were modelled using cable elements with dimensional and material data from the literature, i.e., the anterior SI posterior SI, sacrospinous and sacrotuberous ligaments [26-28]. The new pelvis model was positioned into the existing HBM by matching the acetabula on the femoral heads and adjusting the pelvis to 45° pelvis angle, Fig. 1, which was reported as the average for male subjects in an automotive seated posture [29]. Femoral head ligaments connecting each femur to the acetabulum were modelled with shell elements using non-linear material data of the human hip joint capsule [30], with separate material models for the superior and inferior iliofemoral ligament and the ischiofemoral ligament. The lunate surface of the acetabulum was covered with a 3 mm thick layer of hexahedral solid elements with the same material as the pubic symphysis disc to represent hyaline cartilage, covered with a null-shell which provided the contact definition between the acetabulum and the femoral head.

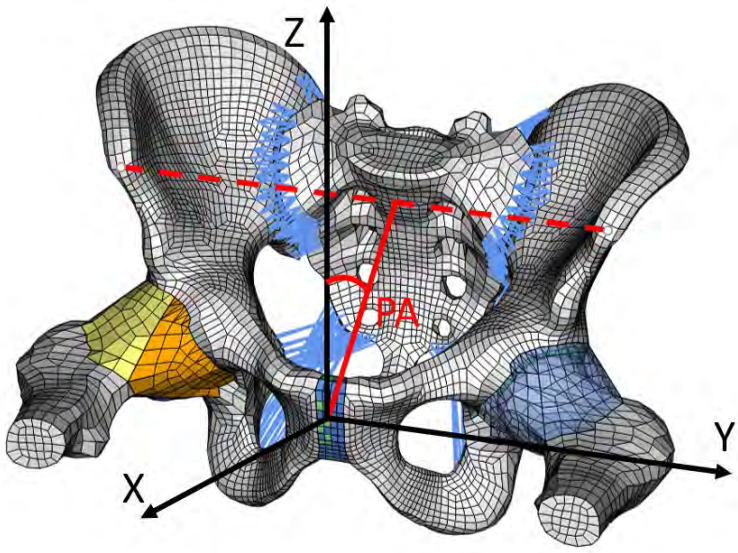

Fig. 1. New pelvis model included in the SAFER HBM v10. The Pelvis Angle (PA), defined as the angle between a vector from the centre of the pubic symphysis to the midpoint between the left and right anterior superior iliac spine and the vertical axis in the XZ-plane of the model, was set to 45° in accordance with the average for seated males in an automotive seat [29]. The yellow part of the femoral head ligament is the superior iliofemoral ligament and the orange the inferior iliofemoral ligament.

The mesh of the subcutaneous soft tissues of the torso and proximal parts of the extremities was updated to fit the new pelvis and to improve the numerical stability when interaction with vehicle interior and restraints. These parts were meshed using hexahedral elements with three elements through the thickness, using a target element side length of 10 mm for the torso and a continuous transition over to the mesh of the extremities. The

internal organs representing the lungs, upper, mid, and lower abdomen were re-meshed as four separate volumes using hexahedral elements with 10 mm characteristic length. The outer surface of the upper thorax and extremities was adapted to that of a statistically based shape representing a 50th percentile male (50 years old, 175 cm and 77 kg) [31]. The soft tissue mesh was divided into two parts, approximately representing the distribution of muscle and adipose tissues, see Fig. 2 (a). Both the muscle and the adipose tissues were represented using hyper-viscoelastic material models [32]. The skin was implemented as a 1 mm thick layer of anisotropic membranes, positioned on the external surface with material directions based on Langer's Line atlas data [33-35], and material properties based on anisotropic non-linear data measured in vivo [36]. The material parameters used for the a-direction were E_c = 22 MPa and CF = 220, and E_c = 6 MPa and CF = 100 [36] for the b-direction (Fig. 2), converted to a second Piola-Kirchoff Stress – Green-strain relation for use in *MAT_FABRIC. The material orientation for the membrane elements, representing the Langer's lines can be seen in Fig. 2 (b).

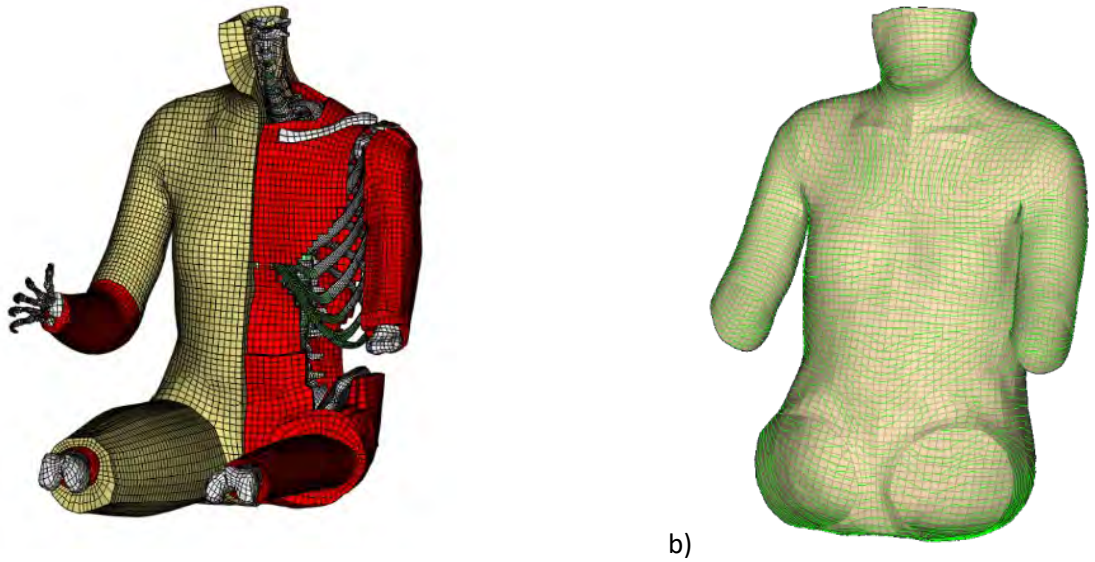

a) b)

Fig. 2 a) New torso and soft tissue mesh with adipose tissue (khaki coloured) and muscle tissue (red). The elbows and lower arms are only modelled with the muscle material model, which was shown to be more numerically stable in near-side impact with intruding structures. b) Skin with mapped material directions [33]. The green lines indicate the stiffer a-direction of the anisotropic skin material model [36], while the less stiff b-direction is perpendicular to the a-direction

The joints of the shoulder girdle were replaced by kinematic joints, as the previous modelling strategy restricted the movement of the shoulder. Additionally, the joint maximum Range of Motion (RoM) was defined based on values reported in literature [37-39]. Within the RoM the resistance was set to a low value (± 1 Nm/RoM) while outside the RoM it was set to a high value (± 3000 Nm/rad), to limit the joint motion. The maximum RoMs implemented with respect to the initial driving posture of the model, Fig. 2, were 3° in depression, 32° in elevation, 16° in retraction, 10° in protraction, 10° in anterior rotation and 40° in posterior rotation for the sternoclavicular joint. For the glenohumeral joint the maximum RoM was defined as, 50° in extension, 115° in flexion, 80° in abduction, 90° in adduction, 135° in medial and 70° in lateral internal rotation. The acromioclavicular joint was defined without any limitations to the RoM.

The radius, ulna, carpals, metacarpals, phalanges, and ligaments were replaced with a new model [40] developed from medical images, ligaments and joints based on literature. The radius, ulna and hand were positioned in a driving posture matching that of the existing lower arm in the SAFER HBM, and soft tissues and skin were added on top of the skeletal structure of the lower arms.

The mesh of the tibia, fibula, calcaneus, and talus of the lower legs were replaced by a pure hexahedral mesh representing the trabecular bone and a quadrilateral shell mesh representing the cortical bone. The updated lower extremity geometry was based on CT-Scans from five females [41] and scaled to fit the 50th percentile male. The cortex of the intermediate bones, metatarsals and phalanges of the feet was modelled using rigid shells, replacing the original mesh, while the original ligaments and soft tissues of the lower legs were kept.

The previous SAFER HBM version had in total 160 contacts, which were reduced to 43 in SAFER HBM v10.

Surface to surface contacts were as far as possible replaced by one general single surface contact, containing the axial skeleton, the thoracic and abdominal cavity and the proximal parts of the extremities. As the torso soft tissues were discontinuous from the skeletal structure, an additional, double defined, sliding-only contact and tied contact to sternum was added in addition to the single-surface contact to avoid cavities forming between the soft tissues and rib cage. For the distal extremities, four single surface contacts were defined, in addition to some specialised surface to surface contacts, for example in the complex knee area. All contacts were modelled using a segment-based contact algorithm (LS-DYNA contact option SOFT=2) and all contacts were ensured free from initial intersections and penetrations.

Simplified Far-Side Impact Validation Set-Up

Reference [12] conducted repeated PMHS oblique (60° from frontal) and far side lateral tests, using a simplified laboratory environment, consisting of a rigid seat, a simplified rigid pelvic restraint and a three-point seatbelt. A subsample of these tests was used in the current validation study. The SAFER HBM was positioned in the average PMHS position [12] in a FE model of the simplified test buck. The seatbelt model D-ring, buckle and outboard anchoring positions were adjusted, to achieve the same belt angles, as the average measured in each configuration. Fig. 3 shows the initial position and belt routing in Configuration 2 for the SAFER HBM and the three PMHSs tested in in the same configuration from [12]. In total, six different configurations, matching those of the PMHS tests in [12] were run with parameter settings as listed in Table I. A constant contact friction coefficient of 0.7 was used for all contacts between the occupant and the seat and seatbelt.

TABLE I

IMPACT CONFIGURATIONS FOR THE SIMPLIFIED FAR-SIDE IMPACT VALIDATION SET-UP.

Configuration	ΔV (km/h)	Impact Direction	D-Ring Position	Pre-tensioner	Pelvic restraint
1	16	Oblique	Intermediate	No	No
2	16	Oblique	Intermediate	Yes	No
3	34	Oblique	Intermediate	Yes	No
4	16	Oblique	Back	Yes	Yes
5	16	Lateral	Forward	Yes	No
6	34	Lateral	Intermediate	Yes	No

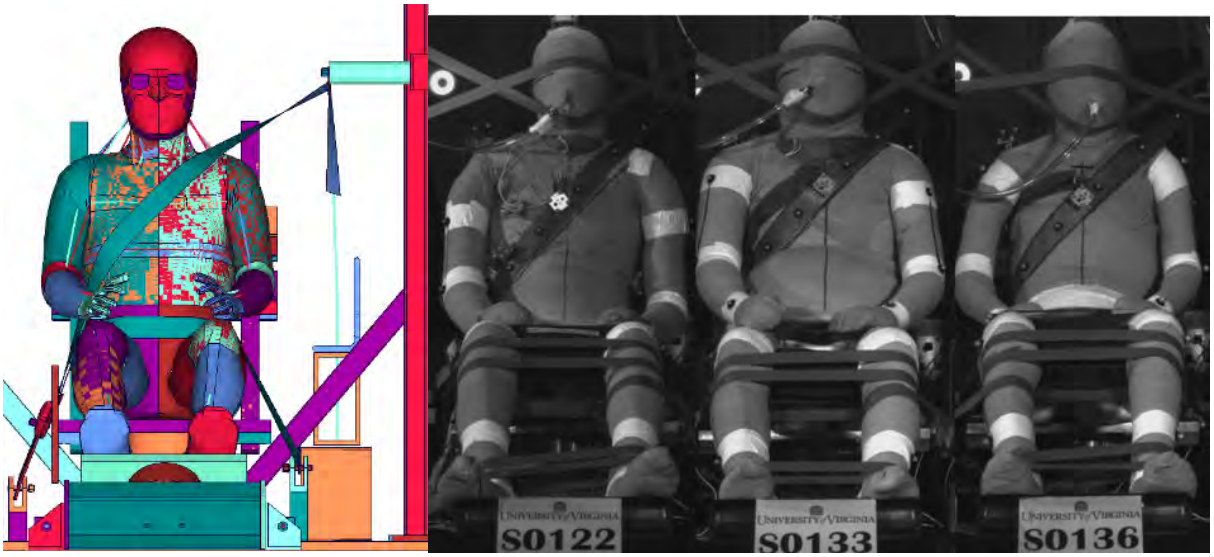

Fig. 3. FE model for the simplified far-side impact validation set-up and the initial position of the SAFER HBM in Configuration 2 (left) and the initial positions of the corresponding three PMHSs in [12] (right) .

The crash pulses for the FE models were defined as the average PMHS pulse for each configuration. The SAFER HBM time history results were compared to PMHS corridors [15] using the method Correlation and Analysis (CORA) [42]. The kinematic signals analysed were; displacements of the head, left and right acromion, T1 and pelvis, as well as lateral lean (difference between T1 and pelvis displacements) and torso twist (difference

between left and right acromion forward excursion), see Table AI in Appendix A. In addition, the predicted shoulder and lap belt forces were compared to the published PMHS test results. For Configuration 1, the simulation was repeated five times with [1,2,3,4,6]x32 central processing units (CPUs) to evaluate the variation due to different decompositions of the FE model [43].

Vehicle-Based Far-Side Impact Validation Set-Up

Reference [18-19] conducted eight PMHS oblique (75° from frontal) far-side impact tests, using a vehicle interior fixture based on a commercially available mid-size sedan (Fig. 4), including driver and passenger seats, a centre console and a three point 2kN force limited belt (2.5 kN measured in upper shoulder belt) Fig. 4. The crash pulse was the same in all tests with a ΔV of 33.5 km/h and peak acceleration of 16 g. In three of the tests a far-side airbag was used (Fig. 5).

As for the simplified set-up, the SAFER HBM was positioned in the average PMHS position (for each test configuration) in an FE model of the vehicle-based buck [32]. The seatbelt, including the webbing, latch, buckle, D-ring and retractor, was adjusted to match the average PMHS belt routing for the two configurations. Two configurations, matching those of the PMHS tests in [18] and [19], respectively, were run with parameter settings as listed in Table II. A total of nine PMHS sled tests were used for the HBM biofidelity investigation; five tests without far-side airbag [18] for Configuration 7, and three tests with the far-side airbag [19] for Configuration 8. It should be noted that in some of the PMHS tests in [18], a metal bracket inside the side bolster was removed. However, as was concluded in [18] this had no effect on the overall kinematics, all the PMHS tests were aggregated and used for comparison to the simulation results in Configuration 7. Similar to the simplified far-side impact set-up, a constant contact friction coefficient of 0.7 was used for HBM to seatbelt and seat contact.

TABLE II

IMPACT CONFIGURATIONS FOR THE VEHICLE-BASED FAR-SIDE IMPACT VALIDATION SET-UP.

Configuration	ΔV (km/h)	Impact direction	Far-side airbag
7	33.5	Oblique	No
8	33.5	Oblique	Yes

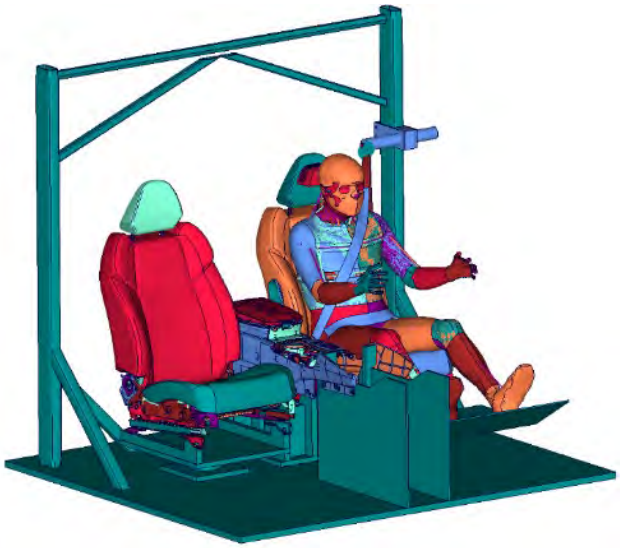

Fig. 4. FE model for the vehicle-based far-side impact validation set-up and initial position of the SAFER HBM, Configurations 7 and 8.

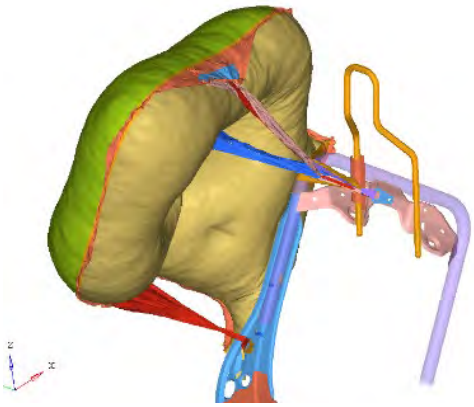

Fig. 5. Far-side airbag model mounted to seat frame, used in Configuration 8.

The SAFER HBM time history results were compared to PMHS corridors, based on the tests in [18] and [19]. The PMHS test corridors were created elaborating on previous techniques [44-45], further described in Appendix B. The updated approach better accounts for possible differences in time-to-peak in the individual responses. The kinematic signals analysed were displacements of the head, shoulder, and sternum, see Table AII in Appendix A. In addition, belt forces and belt pay-out were included in the comparison.

CORA Analysis

Time histories for the measurements were extracted from the simulations and a CORA [42] rating analysis (corridor method using PMHS corridors as inner bounds + cross correlation method on the mean trace of PMHS corridor upper and lower bound) were carried out for each measurement with settings in accordance with Appendix C. The final CORA rating for a signal ranges from 0 to 1, where 0 means no correlation and 1 is perfect correlation. For each configuration, the CORA rating was divided into two parts. The first part was the kinematic HBM response and the second the boundary conditions. The overall CORA score was calculated as the average of the kinematic responses. The ISO/TR 9790 [46] biofidelity rating scale for side-impact dummies (rating 0–10), where a Good biofidelity classification is achieved for a rating ≥6.5/10, was used also for assessment of the HBM. The 0.65 rating level was assumed also to be applicable for HBMs.

III. RESULTS

HBM Updates

The new subcutaneous soft tissues and re-meshed internal organs were checked to the mesh quality criteria according to Table K I (Appendix). As example, more than 98% of the solid elements had Jacobian values above 0.7 and more than 97% of the solid elements had aspect ratio below 3 in the updated model, see Table III. The skeletal structure of the pelvis was more challenging to model, due to the irregular shape and thin sections of the innominate bones, which is why 6.8% of the hexahedral elements had Jacobian values below 0.7 and 9.3% an aspect ratio above 3. The lowest acceptable limit for Jacobian and aspect ratio was set to 0.3 and 10, and no elements in the updated mesh violates these limits.

TABLE III

MESH QUALITY OF THE UPDATED AND SOME EXISTING PARTS OF THE SAFER HBM AFTER IMPLEMENTATION OF THE NEW PELVIS, NEW SUBCUTANEOUS SOFT TISSUES, AND RE-MESHED INTERNAL ORGAN VOLUMES.
TRABECULAR AND CORTICAL BONE OF THE WHOLE MODEL ONLY INCLUDED PARTS WHICH HAVE BEEN MODELLED AS NON-RIGID.

	Number of Elements	Pentas /Trias	Jacobian < 0.7	Aspect Ratio > 3	Pentas /Trias (%)	Jacobian < 0.7 (%)	Aspect Ratio > 3 (%)
Solid Elements							
Subcutaneous soft tissues	67310	2418	1254	2608	3.6	1.9	3.9
Internal organs	10838	448	5	0	4.1	0.0	0.0
Trabecular bone, whole model	97316	2418	12736	6213	2.5	13.1	6.4
Trabecular bone, new pelvis	23320	0	1584	2158	0.0	6.8	9.3
Shell elements							
Skin (membrane)	21640	340	262	374	1.6	1.2	1.7
Cortical bone, whole model	78127	823	1423	296	1.1	1.8	0.4
Cortical bone, new pelvis	10662	0	350	108	0.0	3.3	1.0

Simplified Far-Side Impact Validation Set-Up

For all simplified far-side impact configurations (Configurations 1-6), the boundary conditions were accurately reproduced, indicated by boundary condition CORA scores ranging from 0.83 to 0.92, see Table IV. For all except one of the evaluated configurations, the SAFER HBM also predicted the kinematics of the published PMHS with a kinematic CORA score above 0.65, indicating good biofidelity. For these configurations the overall kinematic CORA scores ranges between 0.73 to 0.78. However, for Configuration 5, with a pure lateral pulse and the D-ring in the forward position, the overall kinematic CORA score was 0.49. A complete list of CORA scores for all signals can be found in Appendix D.

TABLE IV
BIOFIDELITY EVALUATION CORA ANALYSIS GENERIC EVALUATION

Configuration	CORA Rating	
	Belt Forces	Kinematics
1	0.92	0.78
2	0.87	0.73
3	0.91	0.74
4	0.86	0.73
5	0.83	0.49
6	0.87	0.74
Average	0.88	0.70

In addition, the interaction between the shoulder belt and the upper body of the different PMHS was accurately predicted (judged based on if the belt stayed on the shoulder or not) in four of the six configurations. Snapshots showing lateral excursions for these configurations are shown in Appendix E. In Configurations 2-4, the shoulder belt stayed on the shoulder, while in Configuration 1 the shoulder belt slipped off the shoulder, for the SAFER HBM as well as for both PMHS.

In Configurations 1 and 5, the shoulder belt slipped off the shoulder for the SAFER HBM, while it stayed on the shoulder in the corresponding published PMHS tests (Fig. 6 and Fig. 7). Even though these differences in shoulder belt interaction in Configuration 1 (see Fig. 6), the kinematic CORA score was rated as good (0.78).

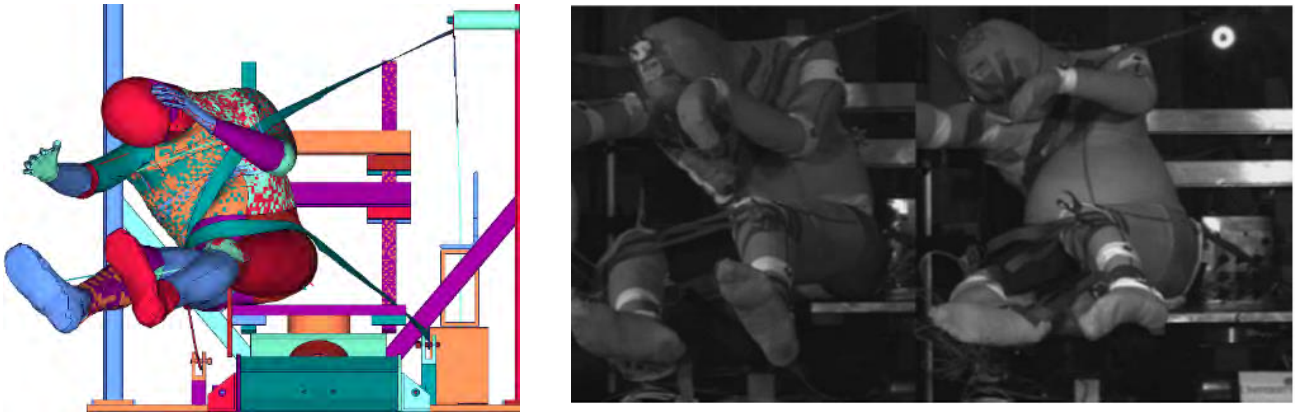

Fig. 6. Simplified far-side impact validation set-up. Snapshots at 120 ms. Configuration 1. SAFER HBM (left) and the two PMHS tests S0124, S0135 from [12].

In Configuration 5, the belt slipped off the shoulder of the SAFER HBM while it remained on the shoulder in the two published PMHS tests, see Fig. 7, resulting in the lowest kinematic CORA score (0.49). The individual signals that gives this low overall kinematic CORA score are the y-displacements of the head (0.53), acromion (Left 0.43/Right 0.45), T1 (0.43) and the z-displacements of the right acromion (0.20) and T1 (0.16). The lack of interaction between the shoulder belt and the torso resulted in torso rotation of the SAFER HBM, while the belt interaction for both PMHS prevented rotation of the upper body to a much higher degree, Fig. 7.

In Configurations 2-4, the peak head lateral excursion was within the PMHS corridor. In Configuration 1, the peak lateral excursion was overpredicted by about 70 mm, in Configuration 6 by about 80 mm and in Configuration 5 by about 200 mm. All time histories used as input to the CORA calculations can be found in Appendix F.

The repeated simulations of Configuration 1, Appendix G, showed a maximum coefficient of variation (CV) of 1.6% for the T1 z-displacement, which varied from 140.4 mm to 146.1 mm in the five simulations. Y-displacements, for instance, had low CV values of 0.23 %, 0.24 % and 0.38 % for the head, T1 vertebra and pelvis, respectively.

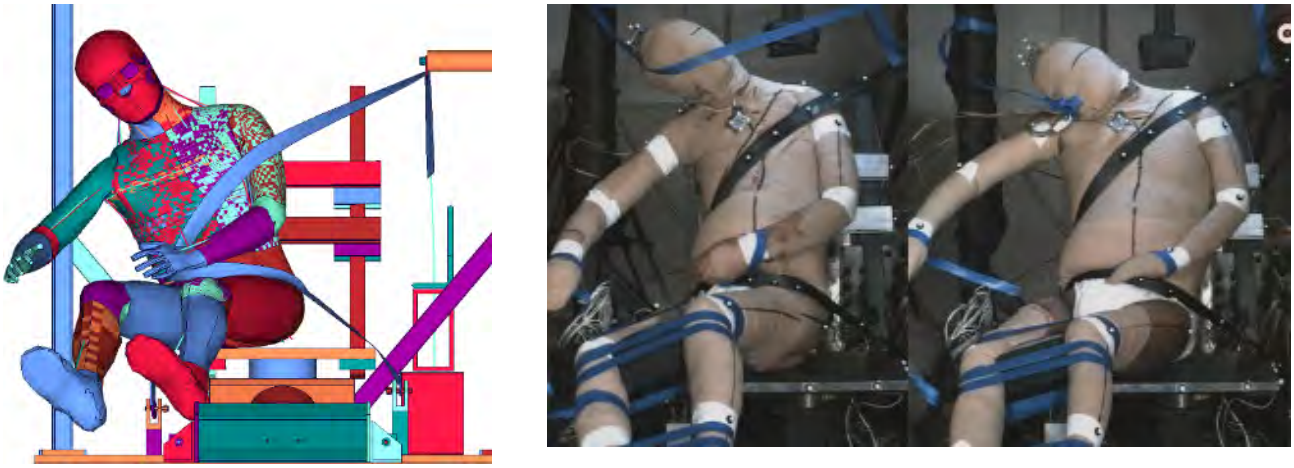

Fig. 7. Simplified far-side impact validation set-up. Snapshot at 140 ms. Configuration 5. SAFER HBM (left) and the two PMHS tests S0083 and S0088 from [12].

Vehicle-Based Far-Side Impact Validation Set-Up

For the vehicle-based set-up, the boundary conditions were accurately reproduced with boundary condition CORA scores of 0.92 (w/o airbag) and 0.79 (w airbag). The kinematics was also predicted with good biofidelity, with kinematic CORA scores of 0.71 (w/o airbag) and 0.65 (w airbag). A complete list of CORA scores for all signals can be found in Appendix H.

The belt to upper body interaction was accurately predicted by the SAFER HBM, as the belt remained on the shoulder for both simulated configurations, similar to the PMHS tests (Fig. 8 and Appendix I). However, the SAFER HBM could not accurately predict the kinematics of the right arm and shoulder, contacting the head in the PMHS tests.

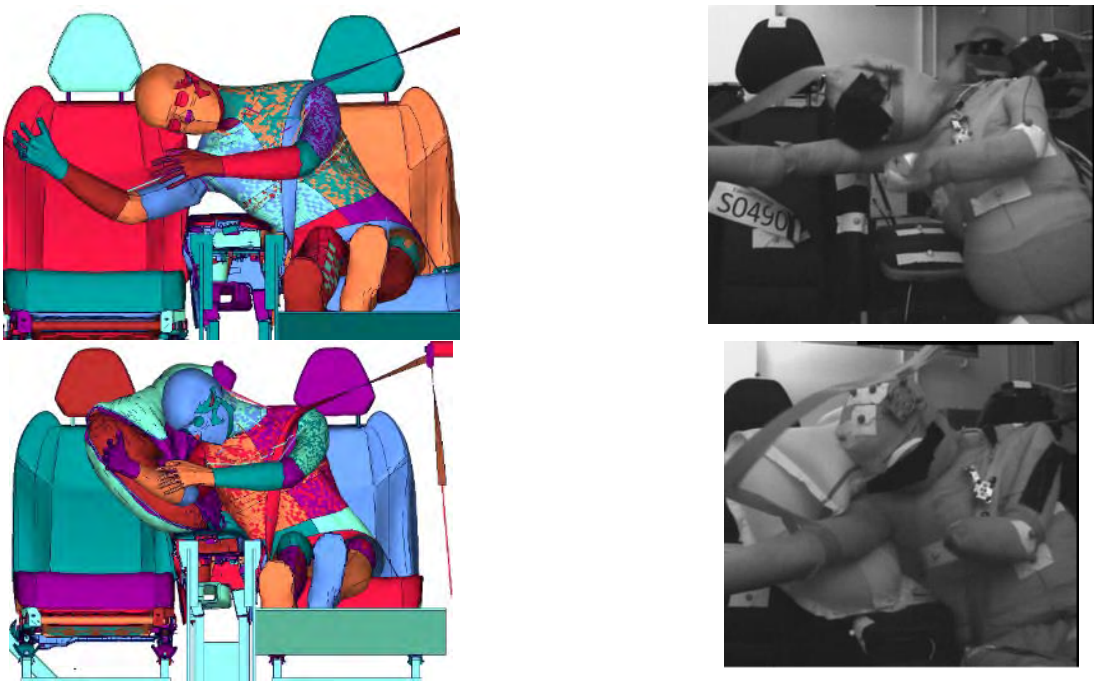

Fig. 8. Vehicle-based far-side impact validation set-up. Configuration 7 without airbag (top) and Configuration 8 with far-side airbag (bottom). SAFER HBM (left) and PMHS from [18-19] (right). Snapshot at 110 ms.

The SAFER HBM overpredicted the head lateral excursion in both configurations. All time histories used as input to the CORA calculations can be found in Appendix J. In the tests without airbag the average head displacement for the five PMHS in the y-direction was approximately 475 mm while the displacement predicted by the HBM was 575 mm. In the tests with an airbag the average head displacement for the three PMHS in the y-direction was approximately 425 mm while the displacement predicted by the HBM was 475 mm. In the PMHS

tests, the far-side airbag reduced head y-displacement by approximately 50 mm while the updated SAFER HBM predicted a reduction of approximately 100 mm. Thereby the updated SAFER HBM confirms the safety benefits of the far-side airbag.

IV. DISCUSSION

In this study the pelvis, torso, upper and lower extremities of the SAFER HBM was updated and evaluated for far-side impact predictions by validation to previously published PMHS tests [12][18-19]. The updated soft tissue mesh had a good quality with more than 97% of the elements meeting the recommendations for Jacobian (>0.7) and aspect ratio (<3) for biomechanics models suggested by [47] and no elements below the minimal limits of 0.3 and 10 for Jacobian and aspect ratio, respectively. The updated pelvis model had a larger part of elements exceeding these recommendations, due to the challenging irregular shape and thin sections of the innominate bones. The updated SAFER HBM was shown capable of recreating occupant kinematics in a total of eight different far-side impact configurations, using two different set-ups with variations in impact direction and occupant boundary conditions, also including a far-side airbag. Other studies, using the same model have shown that the SAFER HBM is a robust and computational efficient HBM [43].

The updated pelvis enables development of the capability of the SAFER HBM to predict pelvis injuries such as iliac wing fractures and other injuries frequently observed in vehicle crashes. In addition, the new pelvis model enables a biofidelic interaction between the lap portion of the belt and pelvis and prediction of pelvis kinematics and sub-marining. The properties of the skin in the updated skin model is considerably softer than the skin properties in previous models. This allows for a more biofidelic interaction between the belt and the skin. The belt can deform the skin and soft tissue that influences the prediction of sliding of the belt across the body. The updated shoulder is important for both the passive and active version of the SAFER HBM. In the active model the upper extremities are activated during an avoidance manoeuvre of the vehicle. The updated upper extremity models were added to enable prediction of fractures of the radius and ulna. Risk curves for prediction of lower arm fracture were developed. The lower extremity models were based on female lower extremity models with corresponding injury risk curves for prediction of calcaneus fractures and soft tissue injuries. The SAFER HBM will continue building on these models and develop risk functions also for males. Morphing of the upper tibia surface was carried out to make the lower extremity models fit the knee joint.

For the simplified far-side impact set-up the model showed overall CORA scores which were marginally different from the validation of a previous version of the model in this set-up [15]. As examples, the combined kinematic and boundary condition CORA score was increased from 0.79 to 0.80 for the updated SAFER HBM in Configuration 1 [15], while for Configuration 5 it was decreased from 0.60 to 0.55. In the updated version of the SAFER HBM the mesh between the arm and shoulder is continuous. However, in previous version of the SAFER HBM the mesh between the arms and shoulder was disjoint. The shoulder and torso mesh were separate. Therefore, when the shoulder was loaded by the belt there was a gap between the upper arm and shoulder. The gap influenced the interaction between the belt and the upper torso. In Configuration 5, with the continuous mesh the belt slip-off occurred earlier, leading to a lower CORA score for continuous mesh compared to for the discontinuous mesh.

Another reason for the low CORA scores for the head in some configurations can be that the tape the holds the head of the PMHS before test was not included in the model [12]. Despite the fact that the tape breaks at low load in some of the PMHS tests it was observed that in some of the tests the head was released late in the event. Therefore, head displacement can be influenced by the presence of the tape.

Previously, the GHBMC simplified model, another HBM, was validated in all the six configurations of the simplified far-side impact set-up [16]. The total CORA for each configuration in that study did not include the right acromion movement, lateral lean and twist, but the range of average CORA scores was 0.47–0.71 for the unmorphed model and 0.58–0.83 for a model morphed to the PMHS anthropometry. Similar to the present study, Configuration 5 gave the lowest total CORA score (0.47), showing that this configuration is challenging to predict with an HBM. As Configuration 5 has the D-ring in a forward position and a pure lateral pulse the occupant response will be largely dependent on retention of the shoulder belt, which was not possible to capture with the HBM in this study. The detailed GHBMC have also been validated in some of the six simplified configurations [14]. CORA scores were not reported in that study. However, when comparing the belt to shoulder interaction, similarities to the current study can be seen. Similar to the SAFER HBM, the detailed GHBMC model in [14] could

retain the belt on the shoulder in Configurations 2 and 3, while the belt slipped off the shoulder in Configuration 1. No comparative data for GHBMC was available for the challenging Configuration 5. Instead two other 16 km/h lateral configurations with the D-ring further rearward were included, and the detailed GHBMCC predicted the belt retention in both cases [14]. The major difference can be seen for Configuration 6, where the detailed GHBMC predicted that the belt should remain on the shoulder, while the belt slipped off the shoulder for the SAFER HBM as well as in the PMHS test. When comparing these studies, the friction coefficient in the contact between the shoulder belt and the HBM should be considered as it will have a large influence on the belt being retained or not by the HBM. In this study a value of 0.7 [15] was used for all simulations, while the study with the simplified GHBMC utilised a friction coefficient of 0.5 [16] and the detailed GHBMC study 0.5 and 0.8 [14].

For the vehicle-based set-up, kinematics CORA scores of 0.71 and 0.65 were achieved for the configurations without and with far-side airbag, respectively. For the vehicle-based set-ups, the SAFER HBM was successful in reproducing the shoulder belt interaction, i.e., the belt stayed on the shoulder in line with the PMHS tests in [18] and [19]. Peak head Y-displacements were overpredicted by the SAFER HBM, but the CORA scores for these signals were highly influenced by the shape of the signal being close to the average signal of the five PMHS. As an example, the head Y-displacement CORA values were 0.96 and 0.92 for Configuration 7 and 8, respectively.

For all PMHS there was an interaction between the shoulder and the head as a result from the arm straightening out in the PMHS tests. The head forward displacement can have been limited by this interaction. This shoulder head interaction was not predicted by the SAFER HBM therefore a greater head x-displacement was predicted with the model.

The influence of the coupling between pelvis, T1 and head on the potential accumulation of the differences in displacements was investigated by evaluating the CORA score for pelvis, T1 and head (Fig. 9 and 10). For Configuration 3 in x-direction there seems to be an accumulation of differences in displacements. The CORA score was reduced from pelvis to T1 to head. However, for Configuration 6 there was an increase in CORA score from pelvis to head. For the other configurations in x-direction and all configurations in y-direction no accumulation of differences in displacements from pelvis to head was observed. Another observation was that generally the CORA score in y-direction was greater than in x-direction.

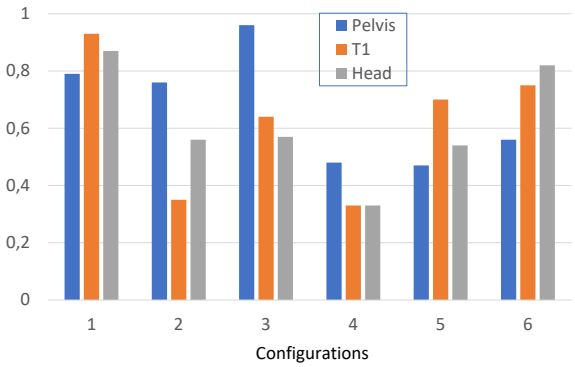

Fig.9. CORA score in x-dir for pelvis, T1 and head for configuration 1-6

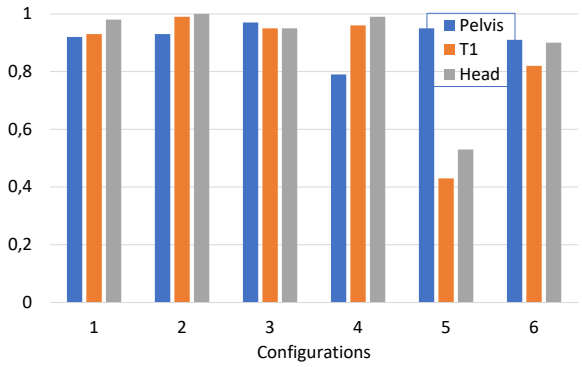

Fig.10. CORA score in y-dir for pelvis, T1 and head for configuration 1-6

As also discussed in [14] and [16] the outer shape of the HBMs differs from the PMHSs. In particular, some PMHSs have a pronounced abdomen, that expands further early in the test. The variability in abdominal shape (between different PMHSs and PMHS to HBM) most likely leads to the variability in shoulder belt to torso interaction seen in Figures C1 and C2 in Appendix E. In some cases, the pronounced abdomen might help to retain the belt on the shoulder as the shoulder belt is pushed upwards. However, this will also change how the belt interacts with the ribcage, which might influence rib fracture risk.

For the model updates, continuous mesh was created, connecting the torso to the shoulder in an attempt to improve the restraint interaction compared with the previous model (which had a disjoint torso and shoulder mesh). Soft material models which gave good numerical stability in the simulated far-side impact set-ups, and in other high severity impacts [43], were used but there still appears to be room for improvement of the shoulder movement in the far-side load case as the non-belted arm of the HBM did not abduct far enough to interact with the head of the occupant as it did for the five PMHS in the vehicle-based validation set-up, Fig. 8. The detailed

GHBMC also uses a continuous mesh connecting the torso to the shoulder, while the simplified GHMBC has a discontinuous mesh. In the far-side validation of the detailed GHBMC model [14] the snapshots indicate that the motion of the non-belted arm is somewhat restricted also for this model. On the other hand, the non-belted arm of the simplified GHBMC is less restricted, indicated by the snapshots in [16]. The reason for that the SAFER HBM arm did not abduct far enough can be that the representation of the soft tissue in the model is stiffer than in the PMHS. Another limitation of the current model is the use of a single surface for the thoraco-abdominal cavity, which does not include any transfer of tension forces through the contacts.

In this study, the calculated CORA scores were divided into averages for the assessed kinematics and for the boundary conditions. The reason for this spilt is that the boundary condition CORA score, does not primarily provide information of the HBM performance, but rather of how well the simulation model such as the belt retractor model was able to reconstruct that of the test environment. Therefore, high boundary condition CORA scores gives confidence in the simulation but would inflate the HBM quality rating if included in the total rating, while low boundary condition CORA scores makes it possible to question the simulation, but does not give any quantitative information about the performance of the assessed HBM.

For the repeated simulations of Configuration 1 in the simplified far-side impact set-up, small CV values (<1.63%, Appendix G) of the responses were found for both peak kinematics and boundary conditions forces. This indicates that for these measurements, the SAFER HBM and the simulation set-ups used were insensitive to variations in the model decomposition which occur with varying number of CPU used for the simulations. This was also shown to be the case for the SAFER HBM in frontal and near-side impacts in a study evaluating the reproducibility of the model, while a near-side oblique impact show more variability [43].

The SAFER HBM was not successful in predicting the shoulder belt to torso interaction in all configurations. In two of the six configurations of the simplified far-side impact set-ups, the shoulder belt slid off the shoulder of the SAFER HBM, while it stayed on the PHMS [12]. The anthropometry of the PMHS can influence the sliding of the shoulder belt over the chest. In the current study, the SAFER HBM used is one size only, whereby representing one individual. To mimic shoulder belt and torso interaction of various PMHSs, there is a need to morph the HBM to the anthropometry of each specific PMHS, such an in [16].

The kinematics of the legs and feet were observed to differ between the SAFER HBM and the PMHS. One reason was that the kinematics of the legs of the PMHS was influenced by foam blocks positioned between the legs. In addition, tape was wrapped around the legs. The foam block and tape were not included in the model due to the fact that in a passenger vehicle, the motion of the legs and feet are limited by the vehicle interior. In addition, modelling the foam block and tape was not considered since the documentation was not at a level of detail necessary for modelling. Therefore, no correlation analysis was carried out for the kinematics of the SAFER HBM lower extremities.

The tilting of the PMHS and the SAFER HBM was assessed in the measure “lateral lean”. It can be observed that “lateral lean” was predicted by the SAFER HBM for Configuration 2,3 and 4. For Configuration 1, 5 and 6 “lateral lean” is overpredicted with the model. Therefore, no trend that the SAFER HBM predicts more lateral lean than that what was obtained in the PMHS tests was observed.

The present study included a large span of far-side impact variations, including impact direction and occupant boundary conditions. The SAFER HBM is robust and generally the model predicted the kinematics from published PHMS tests in most of the configurations. This capability is of importance when assessing countermeasures, such as the ambitions for virtual testing by Euro NCAP as part of their roadmap for future protocols [9]. Far-side airbags, as included as one of the configurations in this study, are examples of such countermeasure. The model development, and the whole-body validation as presented in this study, can help support the development of real-world relevant occupant protection in far-side impacts.

A broader validation of the SAFER HBM at both component and full body level by means of different loadcases is ongoing. The level of validation of the model will be evaluated in frontal, oblique and side impact load cases. In addition, validation of the model for reclined seating positions is ongoing.

Sub-system validation of the lumbar and cervical spine was presented in [48] and showed that the properties of the lumbar spine, which influences the whole-body kinematics in far-side impacts, was matching PMHS well for lateral shear, but overly flexible in lateral bending. The new soft tissues included in the model updates in this paper is likely to rebalance the load distribution from the soft tissues which previously was stiffer in the whole body HBM to the lumbar spine.

.

V. CONCLUSIONS

The updated SAFER HBM (version 10) was validated in two far-side impact set-ups; one simplified and one vehicle-based environment, with variations of impact direction and occupant boundary conditions, also including a far-side airbag. The SAFER HBM was able to predict the occupant shoulder belt interaction in six of the eight simulated configurations with CORA scores of 0.65–0.74 for the evaluated kinematic variables. In two of the simplified configurations, the SAFER HBM slid out of the belt while all PMHS in the corresponding published tests did not. Far-side kinematics and boundary condition forces were found to be insensitive to the model decomposition with low coefficient of variation of peak values for repeated simulations with varying numbers of CPU.

VI. ACKNOWLEDGEMENT

This work was carried out at SAFER, Vehicle and Traffic Safety Centre at Chalmers University of Technology, Gothenburg, Sweden, and funded by FFI-Strategic Vehicle Research and Innovation, by Vinnova, the Swedish Energy Agency, the Swedish Transport Administration and the Swedish vehicle industry. Part of the simulations were performed on resources at Chalmers Centre for Computational Science and Engineering (C3SE) provided by the Swedish National Infrastructure for Computing (SNIC).

VII. REFERENCES

[1] Gabler C, Fitzharris M, Scully J, Fildes BN, Digges K, Sparke L (2005) Far side injury risk for belted in Australia and the United States. *19th International Technical Conference on the Enhanced Safety of Vehicles Conference (ESV)*, June 2005, Washington DC, USA.

[2] Yoganandan N, Arun MWJ, Halloway DE, Pintar FA et al. (2014) Crash characteristics and injury patterns of restrained front seat occupants in far-side impacts. *Traffic Injury Prevention,* 15:sup1, S27-S34, DOI: 10.1080/15389588.2014.935771

[3] Fildes B, Vulcan P, Lane J, Lenard A (1994) Side impact crashes in Australia. *14th International Technical Conference on the Enhanced Safety of Vehicles Conference (ESV)*, 94-S6-O-01, May 1994, Munich, Germany.

[4] Bahouth GT, Muakhovskiy D, Digges KH, Rist H, Wiik R (2015) Opportunities for reducing far-side casualties. *24th International Technical Conference on the Enhanced Safety of Vehicles Conference (ESV)*, June 2015, Gothenburg, Sweden.

[5] Mackay GM, Hill J, Parkin S, Munns JAR (1993). Restrained occupants on the nonstruck side in lateral collisions. *Accident Analysis & Prevention*, 25:147-152.

[6] Bostrom O, Gabler HC, Digges K, Fildes B, Sunnevang C. (2008) Injury reduction opportunities of far side impact countermeasures. *Ann Adv Automot Med*, 52: 289-300.

[7] Newland C, Belcher T et al. (2008) Occupant-to-occupant interaction and impact injury risk in side impact crashes. *Stapp Car Crash Journal*, 52: 327-347.

[8] Euro NCAP Far side occupant test & assessment procedure version 1.0., *European New Car Assessment Programme*, Antwerp, the Netherlands. https://cdn.euroncap.com/media/32284/euro-ncap-far-side-test-and-assessment-protocol-v10.pdf (accessed: 2021-04-01).

[9] van Ratingen M (2020) Update on Virtual Testing in safety assessment of new vehicles from Euro NCAP. *IRCOBI pre-conference workshop "VIRTUAL-OSCCAR Workshop: Progress in Virtual Testing for automotive applications"*, 8 September 2020, online.

[10] Fildes BN, Spake LJ, Bostrom O, Pintar F, Yoganandan N, Morris AP. (2002) Suitability of current side impact test dummies in far-side impacts. *Proceedings of IRCOBI Conference*, Sept 2002, Munich, Germany.

[11] Pintar F, Yoganandan N et al. (2007) Comparison of PMHS, WorldSID, and THOR- NT responses in simulated far side impact. *Stapp Car Crash Journal*, 51: 313-60.

[12] Forman J, Lopez-Valdes F et al. (2013) Occupant kinematics and shoulder belt retention in far-side lateral and oblique collisions: A Parametric Study. *Stapp Car Crash Journal*, 57: 343-385.

[13] Perez-Rapela D, Markusic C et al. (2018) Comparison of WorldSID to PMHS kinematics in far-side impact. IRC-18-91. *Proceedings of IRCOBI Conference*, Sept 2018, Athens, Greece.

[14] Katagiri M, Zhao J, Kerrigan J, Kent R, Forman J. (2016) Comparison of whole-body kinematic behavior of the GHBMC occupant model. *Proceedings of IRCOBI Conference*, Sept 2016, Malaga, Spain.

[15] Pipkorn B, Larsson K-J et al. (2018) Occupant protection in far-side impacts. *Proceedings of IRCOBI Conference*, Sept 2018, Athens, Greece.

[16]Perez-Rapela D, Markusic C, Whitcomb B, Pipkorn B, Forman JL, Crandall JR (2019) Comparison of the simplified GHBMC to PMHS kinematics in far-side Impact. *Proceedings of IRCOBI Conference*, Sept 2019, Florence, Italy.

[17]Petit P, Trosseille X et al. (2019) Far side impact injury threshold recommendations based on 6 paired WorldSID/post mortem human subjects tests. *Stapp Car Crash Journal*. 63: 127–146.

[18]Perez-Rapela D, Donlon J-P et al. (2019) PMHS and WorldSID kinematic and injury response in far-side events in a vehicle-based test environment. *Stapp Car Crash Journal*, 63: 83–126.

[19]Perez-Rapela D, Donlon J-P et al. (2021) Occupant restraint in far-side impacts: Cadaveric and WorldSID responses to a far-side airbag. *Ann Biomed Eng* 49: 802–811.

[20]Iraeus J, Pipkorn B. (2019) Development and validation of a generic Finite Element ribcage for strain based fracture prediction. *Proceedings of IRCOBI Conference*, Sept 2019, Florence, Italy.

[21]Kleiven S. (2007) Predictors for traumatic brain injuries evaluated through accident reconstructions. *Stapp Car Crash Journal* 51, 2007-P-401.

[22]Östh J, Bohman K, Jakobsson L (2020) Evaluation of kinematics and restraint interaction when repositioning a driver from a reclined to an upright position prior to frontal impact using active Human Body Model simulations, *Proceedings of IRCOBI Conference*, Sept 2020, online.

[23]Östh J, Brolin K, Bråse D (2015) A Human Body Model with active muscles for simulation of pretensioned restraints in autonomous braking interventions. *Traffic Injury Prevention*, 16(3): 304–313.

[24]Larsson E, Iraeus J et al. (2019) Active Human Body Model Predictions Compared to Volunteer Response in Experiments with Braking, Lane Change, and Combined Manoeuvres. *Proceedings of IRCOBI Conference*, Sept 2019, Florence, Italy.

[25]Li Z, Alonso J E, Kim J, Davidson J S, Etheridge B S, Eberhardt A W. (2006) Three-dimensional Finite Element models of the human pubic symphysis with viscohyperelastic soft tissues. *Ann Biomed Eng* 34: 1452–1462.

[26]Steinke H, Hammer N et al. (2010) Novel insights into the sacroiliac joint ligaments. *Spine* 35(3): 257-263

[27]Hammer N, Steinke H et al. (2009) The sacrotuberous and the sacrospinous ligament--a virtual reconstruction. *Annals of Anatomy* 191(4): 417-425

[28]Ivanov A, Kiapour A, Ebraheim N A, Goel V. (2009) Lumbar fusion leads to increases in angular motion and stress across sacroiliac joint: A Finite Element study. *Spine* 34(5): E162-E169

[29]Izuiyama T, Nishida N, et al. (2018) The analysis of an individual difference in human skeletal alignment in seated posture and occupant behavior using HBMs. *Proceedings of IRCOBI Conference*, Sept 2018, Athens, Greece.

[30]Hewitt JD, Glisson RR, Guilak F, Parker Vail T (2002) The mechanical properties of the human hip capsule ligaments. *The Journal of Arthroplasty* 17(1): 82–89.

[31]Reed MP, Ebert SM (2013). Elderly occupants: posture, body shape, and belt fit. Report Number: UMTRI-2013-26, *University of Michigan Transportation Research Institute*, Ann Arbor (MI), USA.

[32]Hedenstierna S, Halldin P, Brolin K (2008) Evaluation of a combination of continuum and truss Finite Elements in a model of passive and active muscle tissue. *Computer Methods in Biomechanics and Biomedical Engineering* 11(6): 627–639.

[33]McIntosh L, Fyfe AHB (2013) A7 skine lines and wound healing. *In: Carachi R, Agarwala S, Bradnock TJ, Lim Tan H, Cascio S (eds.) Basic Techniques in Pediatric Surgery*. Springer, Berlin.

[34]Ni Annaidh A, Bruyere K, Destrade M, Gilchrist MD, Ottenio M (2012) Characterization of the anisotropic properties of excised human skin. *J Mech Behav Biomed Mater* 5(1): 139–148.

[35]Ridge MD, Wright V (1966) The directional effects of skin: A bio-engineering study of skin with particular reference to Langer's lines. *Journal of Investigative Dermatology* 46(4): 341–346.

[36]Manschot JFM, Brakkee AJM (1988) The measurement and modelling of the mechanical properties of human skin in vivo – II. The Model. *Journal of Biomechanics* 19(7): 517–521.

[37]Ludewig PM, Phadke V, Braman JP, Hassett DR, Cieminski CJ, LaPrade RF (2009) Motion of the shoulder complex during multiplanar elevation. *The Journal of Bone and Joint Surgery*, 91: 378–89.

[38]Inman VT, Saunders M, Abbott LC (1944) Observations on the function of the shoulder joint. *The Journal of Bone and Joint Surgery* 26(1): 1–30.

[39]Standring S. (ed.) (2008) Gray's Anatomy – The Anatomical Basis of Clinical Practice. Elsevier Churchill Livingstone, London, UK.

[40]Bayat M, Pongpairote N (2020), Arm injury prediction with THUMS SAFER - Improvements of the THUMS SAFER upper extremity, Master Thesis, Royal Institute of Technology (KTH), Stockholm, Sweden. https://www.diva-portal.org/smash/record.jsf?pid=diva2%3A1478959&dswid=5834

[41]Roberts C. (2020) Sex-based geometric differences in the lower extremity and their effect on injury in the automotive crash environment. *PhD Thesis,* University of Virginia, Mechanical and Aerospace Engineering – School of Engineering and Applied Science, Charlottesville (VA) USA, https://doi.org/10.18130/v3-p7nn-n282

[42]Gehre C, Gades H, Wernicke P (2009) Objective rating of signals using test and simulation responses. *21th International Technical Conference on the Enhanced Safety of Vehicles Conference (ESV)*, June 2009, Stuttgart, Germany.

[43]Östh J, Pipkorn B, Forsberg J, Iraeus J (2021) Numerical reproducibility of Human Body Model crash simulations*. Paper submitted to IRCOBI Conference*.

[44]Lessley D, Crandall J, Shaw G, Kent R, Funk J. (2004) A normalization technique for developing corridors from individual subject responses. *SAE Technical paper 2004-01-0288*.

[45]Shaw JM, Herriott RG, McFadden JD, Donnelly BR, Bolte JH (2006) Oblique and lateral impact response of the PMHS thorax. *Stapp Car Crash J* 50: 147-67.

[46]International Organization for Standardization (1999) Technical Report 9790; Road Vehicles; Anthropomorphic side impact dummy - lateral impact response requirements to assess the biofidelity of the dummy. IOS, Geneva.

[47]Burkhart TA, Andrews DM, Dunnin CE (2013) Finite element modeling mesh quality, energy balance and validation methods: A Review with recommendations associated with the modeling of bone tissue. *J Biomech* 46(9): 1477–1488.

[48]Östh J, Bohman K, Jakobsson L (2020) Evaluation of Kinematics and Restraint Interaction when Repositioning a Driver from a Reclined to an Upright Position Prior to Frontal Impact using Active Human Body Model Simulations. *Proceedings of IRCOBI Conference*, Sept 2020, Munich, Germany

VIII. APPENDIX

A. Measurements used for Creating PMHS Corridors

TABLE A I
MEASUREMENTS USED FOR CREATING PMHS CORRIDORS FOR THE SIMPLIFIED FAR-SIDE TEST CONFIGURATION.

Measurement	Component 1	Component 2	Component 3	Unit
Head displacement	X	Y	Z	mm
Left Acromion displacement	X	Y	Z	mm
Right Acromion displacement	X	Y	Z	mm
T1 displacement	X	Y	Z	mm
Pelvis displacement	X	Y	Z	mm
Belt Forces	Shoulder	Lap	Side	N
Thorax	Lateral Lean	Torso Twist	-	Degrees

TABLE A II
MEASUREMENTS USED FOR CREATING PMHS CORRIDORS FOR THE VEHICLE-BASED FAR-SIDE TEST SET-UP.

Measurement	Component 1	Component 2	Component 3	Unit
Head displacement	X	Y	Z	mm
Shoulder	X	Y	Z	mm
Sternum	X	Y	Z	mm
Belt Forces	Shoulder	Lap	Side	N
Belt Payout	Payout	-	-	mm
Console displacement	-	Y	-	mm
Head restraint displacement	-	Y	-	mm

B. Method for PMHS Corridor Calculation for the Vehicle-Based Far-Side Impact Validation Set-Up

The individual time history results of the PMHS tests used for the vehicle-based far-side impact set-ups (Configurations 7 and 8) were published in [18] and [19], respectively. Based on these, the PMHS corridors were created elaborating on previous techniques [44-45] as shown in Fig. B 1.

Firstly, each curve it parametrised by its arc-length, with the arc-length along the curve normalised based on the arc-length between two characteristic points on the curve, i.e., from the value at time 0 ms to the peak value, Fig. B1, a and b). Secondly, the mean and standard deviations in each axis are calculated, i.e., time and displacement) for each step in arc-length (Fig. B1, c and d). Thirdly, the corridors are defined as the set of ellipses with centres at each step in arc-length along the mean curve and semi-axes proportional to the standard deviation in each axis at each step in arc-length (Fig.B1 , e and f).

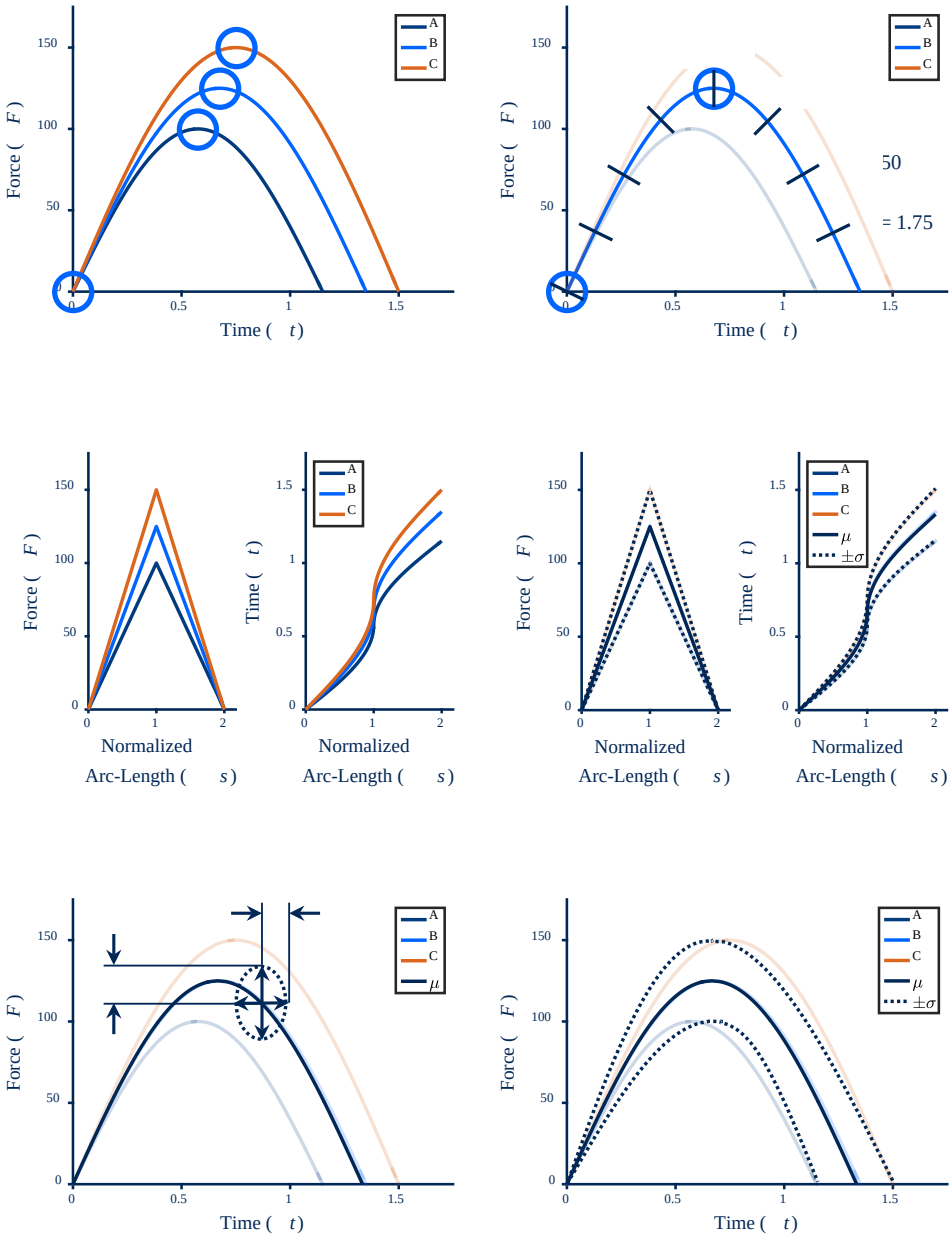

Fig. B 1. Illustration of parametrisation (a, b, c) and corridor creation (d, e, f) for an example data set (individual force time-histories A, B and C). The mean (μ) and standard deviation (σ) were calculated for force (F) and time (t) separately as functions of normalised arc-length (s).

C. CORA Evaluation Parameter Settings, HBM Predictions and PMHS Corridors with CORA Rating

TABLE C I
CORA SETTINGS

CORRIDOR RATING	0.5
CROSS-CORRELATION RATING	0.5
SHAPE	0.5
SIZE	0.25
PHASE-SHIFT	0.25

TABLE C II
CORA PARAMETER SETTINGS USED FOR ALL CORA RATINGS

	Parameter	Setting	Explanation
Time Interval Settings	A_THRES	0.03	Threshold to set the start of the interval of evaluation
	B_THRES	0.075	Threshold to set the end of the interval of evaluation
	A_EVAL	0.01	Extension of the interval of evaluation
	B_DELTA_END	0.001	Additional parameter to shorten the interval of evaluation
	T_MIN/ T_MAX	auto/auto	Start time and end time of the interval of evaluation (automatic = calculated for each channel)
Corridor Method	K	2	Transition between ratings of 1 and 0 of the corridor method
	G_1	0.5	Weighting factor of the corridor method
	a_0/b_0	0.05/ 0.50	Width of the inner and outer corridors
	a_sigma/ b_sigma	1/1	Multiples of the standard deviation to widen the inner and outer corridors
Cross-Correlation Method	D_MIN	0.01	delta_min as share of the interval of evaluation
	D_MAX	0.12	delta_max as share of the interval of evaluation
	INT_MIN	0.80	Minimum overlap of the interval
	K_V	10	Transition between ratings of 1 and 0 of the progression rating
	K_G	1	Transition between ratings of 1 and 0 of the size rating
	K_P	1	Transition between ratings of 1 and 0 of the phase shift rating
	G_V	0.50	Weighting factors of the progression rating
	G_G	0.25	Weighting factors of the size rating
	G_P	0.25	Weighting factors of the phase shift rating
	G_2	0.50	Weighting factors of the cross-correlation method

D. Simplified Far-Side Impact Validation Set-Up; CORA Scores

TABLE D I

CORA SCORES FOR EACH INDIVIDUAL COMPONENT FOR THE SIMPLIFIED FAR-SIDE IMPACT VALIDATION SET-UP

Configuration 1		Configuration 2		Configuration 3		Configuration 4		Configuration 5		Configuration 6	
Head X	0.87	*Head X*	0.56	*Head X*	0.57	*Head X*	0.33	*Head X*	0.54	*Head X*	0.82
Head Y	0.98	*Head Y*	1	*Head Y*	0.95	*Head Y*	0.99	*Head Y*	0.53	*Head Y*	0.9
Head Z	0.66	*Head Z*	0.6	*Head Z*	0.55	*Head Z*	0.79	*Head Z*	0.48	*Head Z*	0.64
LAc X	0.56	*LAc X*	0.44	*LAc X*	0.79	*LAc X*	0.84	*LAc X*	0.84	*LAc X*	0.8
LAc Y	0.88	*LAc Y*	0.98	*LAc Y*	0.96	*LAc Y*	0.95	*LAc Y*	0.43	*LAc Y*	0.89
LAc Z	0.46	*LAc Z*	0.58	*LAc Z*	0.17	*LAc Z*	0.52	*LAc Z*	0.43	*LAc Z*	0.21
Lap Belt Force	0.94	*Lap Belt Force*	0.77	*Lap Belt Force*	0.95	*Lap Belt Force*	0.9	*Lap Belt Force*	0.88	*Lap Belt Force*	0.82
Pelvis X	0.79	*Pelvis X*	0.76	*Pelvis X*	0.96	*Pelvis X*	0.48	*Pelvis X*	0.47	*Pelvis X*	0.56
Pelvis Y	0.92	*Pelvis Y*	0.93	*Pelvis Y*	0.97	*Pelvis Y*	0.79	*Pelvis Y*	0.95	*Pelvis Y*	0.91
Pelvis Z	0.79	*Pelvis Z*	0.64	*Pelvis Z*	0.57	*Pelvis Z*	0.46	*Pelvis Z*	0.35	*Pelvis Z*	0.51
RAc X	0.86	*RAc X*	0.58	*RAc X*	0.89	*RAc X*	0.71	*RAc X*	0.68	*RAc X*	0.68
RAc Y	0.89	*RAc Y*	0.99	*RAc Y*	0.97	*RAc Y*	0.92	*RAc Y*	0.45	*RAc Y*	0.92
RAc Z	0.59	*RAc Z*	0.42	*RAc Z*	0.36	*RAc Z*	0.78	*RAc Z*	0.2	*RAc Z*	0.84
Shldr Belt Force	0.88	*Shldr Belt Force*	0.95	*Shldr Belt Force*	0.94	*Shldr Belt Force*	0.87	*Shldr Belt Force*	0.83	*Shldr Belt Force*	0.93
Side Belt Force	0.95	*Side Belt Force*	0.89	*Side Belt Force*	0.84	*Side Belt Force*	0.82	*Side Belt Force*	0.78	*Side Belt Force*	0.85
T1 X	0.93	*T1 X*	0.35	*T1 X*	0.64	*T1 X*	0.33	*T1 X*	0.7	*T1 X*	0.75
T1 Y	0.93	*T1 Y*	0.99	*T1 Y*	0.95	*T1 Y*	0.96	*T1 Y*	0.43	*T1 Y*	0.82
T1 Z	0.66	*T1 Z*	0.85	*T1 Z*	0.47	*T1 Z*	0.81	*T1 Z*	0.16	*T1 Z*	0.96
Lateral Lean	0.86	*Lateral Lean*	0.97	*Lateral Lean*	0.96	*Lateral Lean*	0.98	*Lateral Lean*	0.44	*Lateral Lean*	0.65
Torso Twist	0.57	*Torso Twist*	0.82	*Torso Twist*	0.9	*Torso Twist*	0.78	*Torso Twist*	0.35	*Torso Twist*	0.64
Belt forces	0.92	*Belt forces*	0.87	*Belt forces*	0.91	*Belt forces*	0.86	*Belt forces*	0.83	*Belt forces*	0.87
Kinematics	0.78	*Kinematics*	0.73	*Kinematics*	0.74	*Kinematics*	0.73	*Kinematics*	0.50	*Kinematics*	0.74
Overall	0.8	*Overall*	0.75	*Overall*	0.77	*Overall*	0.75	*Overall*	0.55	*Overall*	0.76

E. Simplified Far-Side Impact Set-Up: Comparing Snapshots at 140 ms for SAFER HBM and PMHS [12]

Fig. E 1. Test Configuration 2: SAFER HBM (left) and the three PMHS tests S0122, S0133, S0136 from [12] (right)

Fig. E 2. Test Configuration 3: SAFER HBM (left) and the three PMHS tests S0123, S0134, S0137 from [12] (right)

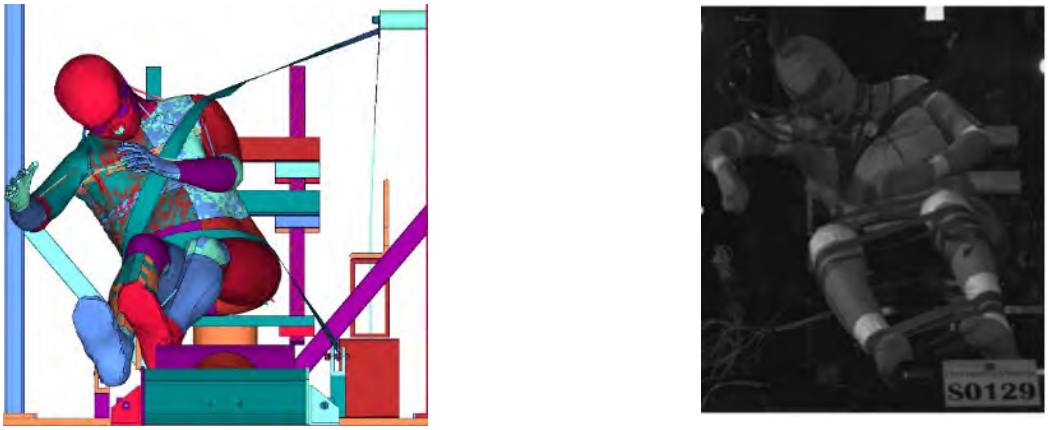

Fig. E 3. Test Configuration 4: SAFER HBM (left) and the PMHS test S0129 from [12] (right)

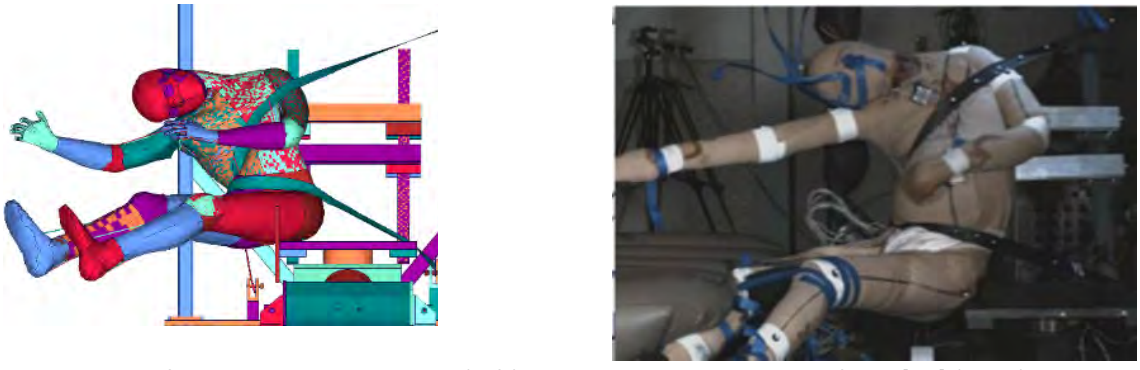

Fig. E 4. Test configuration 6: SAFER HBM (left) and the PMHS test S0091 from [12] (right)

F. Simplified Far-Side Impact Set-Up; SAFER HBM Responses and PMHS Corridors from tests in [12]

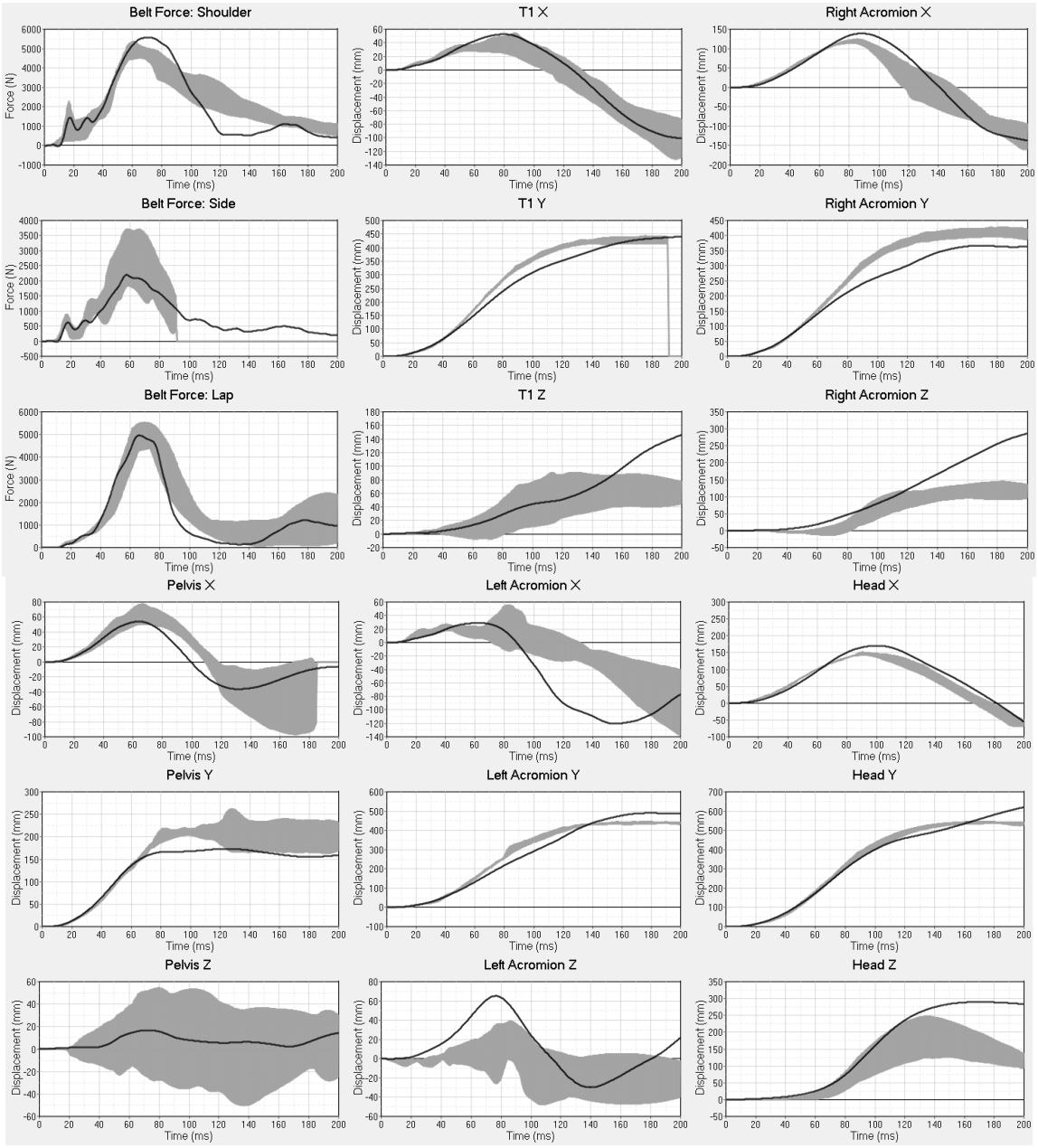

Fig. F 1. HBM responses and corridors from PMHS tests in [12], Configuration 1: Belt forces and kinematic signals.

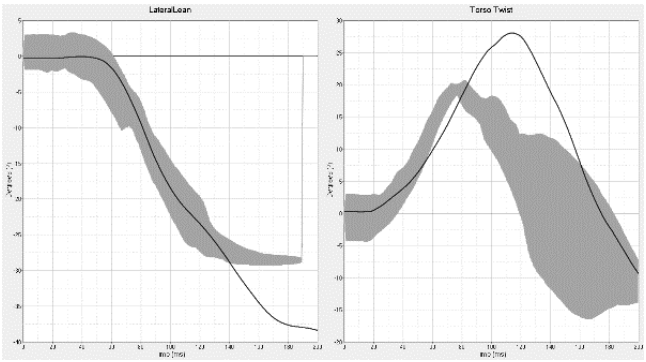

Fig. F 2. HBM responses and corridors from PMHS tests in [12] in, Configuration 1: Lateral lean and torso twist signals.

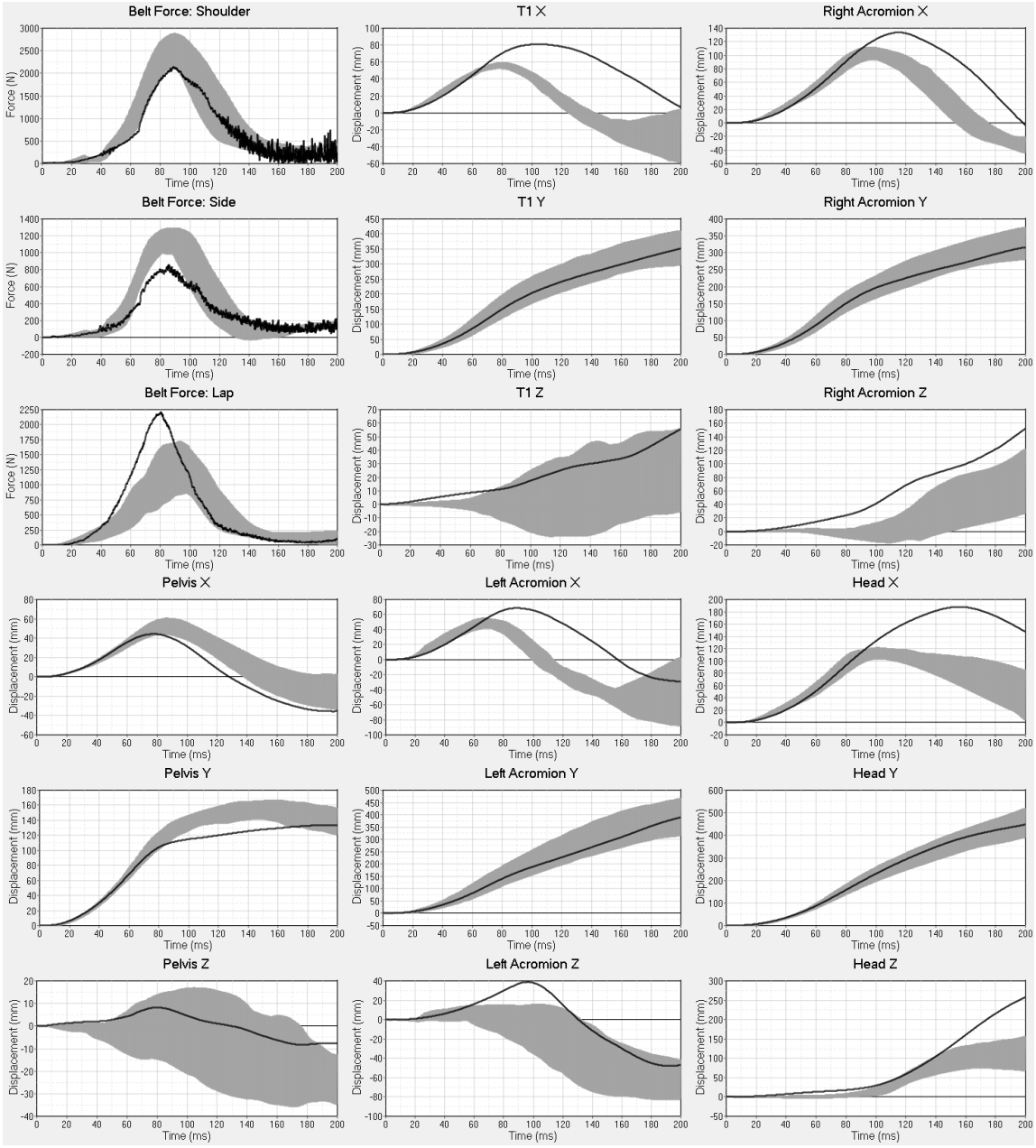

Fig. F 3. HBM responses and corridors from PMHS tests in [12], Configuration 2: Belt forces and kinematic signals.

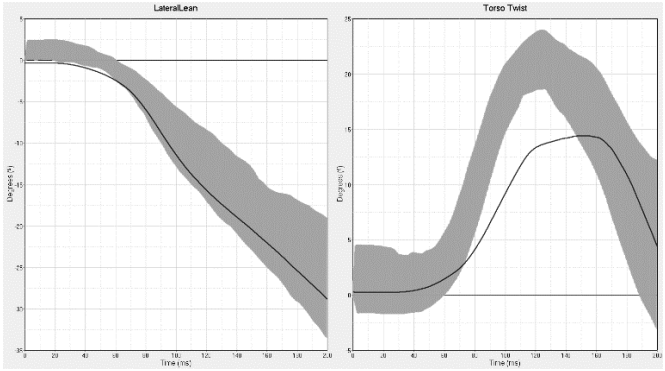

Fig. F 4. HBM responses and corridors from PMHS tests in [12], Configuration 2: Lateral lean and torso twist signals.

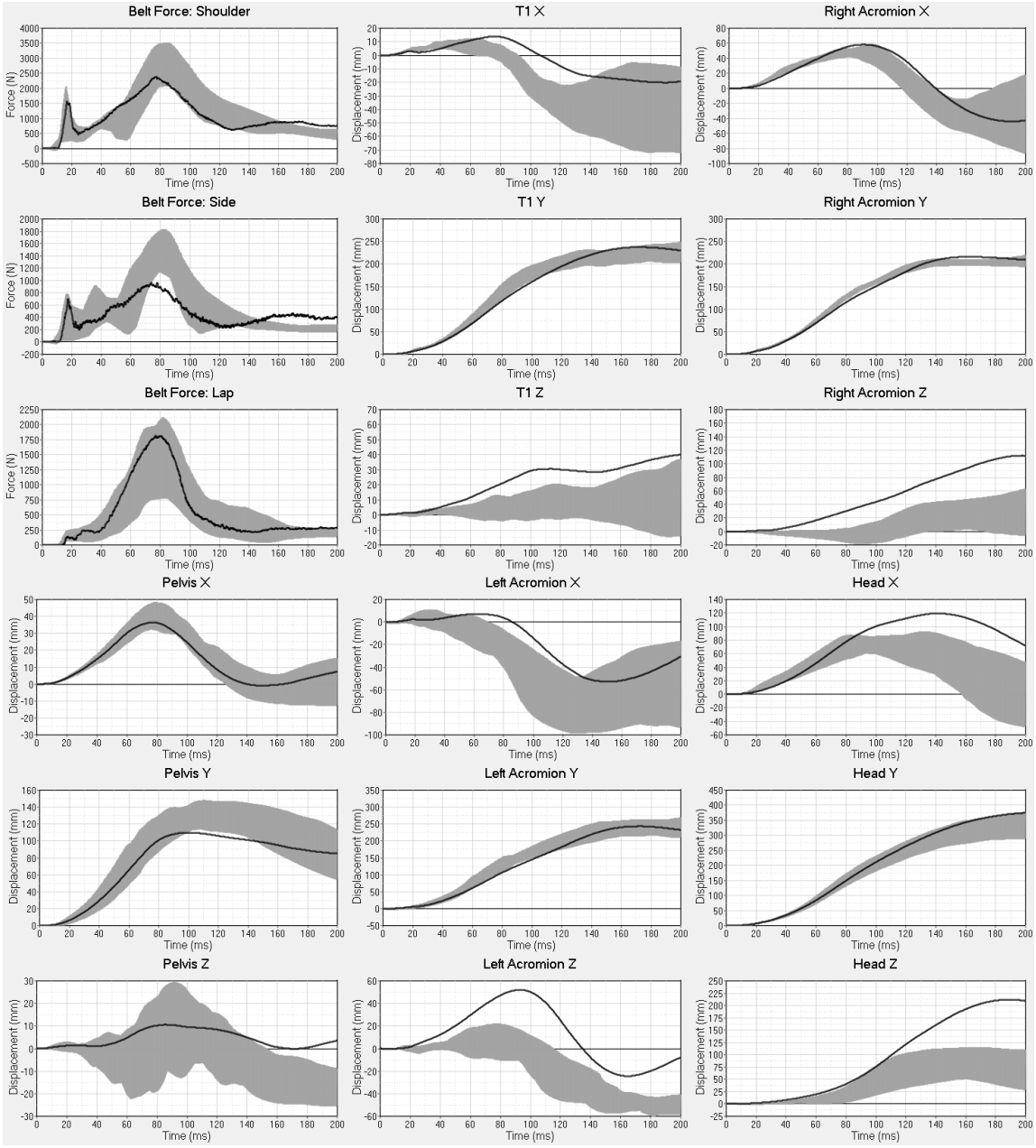

Fig. F 5. HBM responses and corridors from PMHS tests in [12], Configuration 3: Belt forces and kinematic signals.

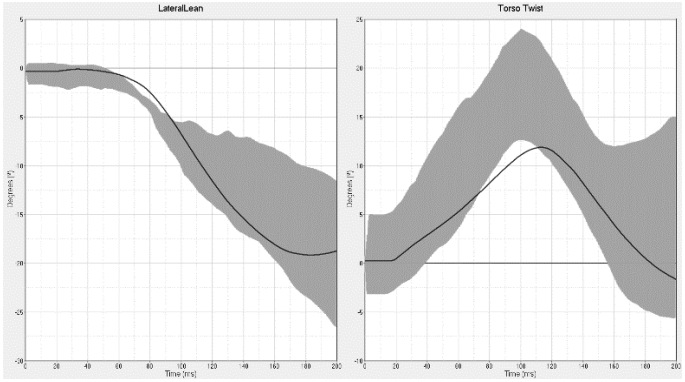

Fig. F 6. HBM responses and validation corridors from PMHS tests in [12], Configuration 3: Lateral lean and torso twist signals.

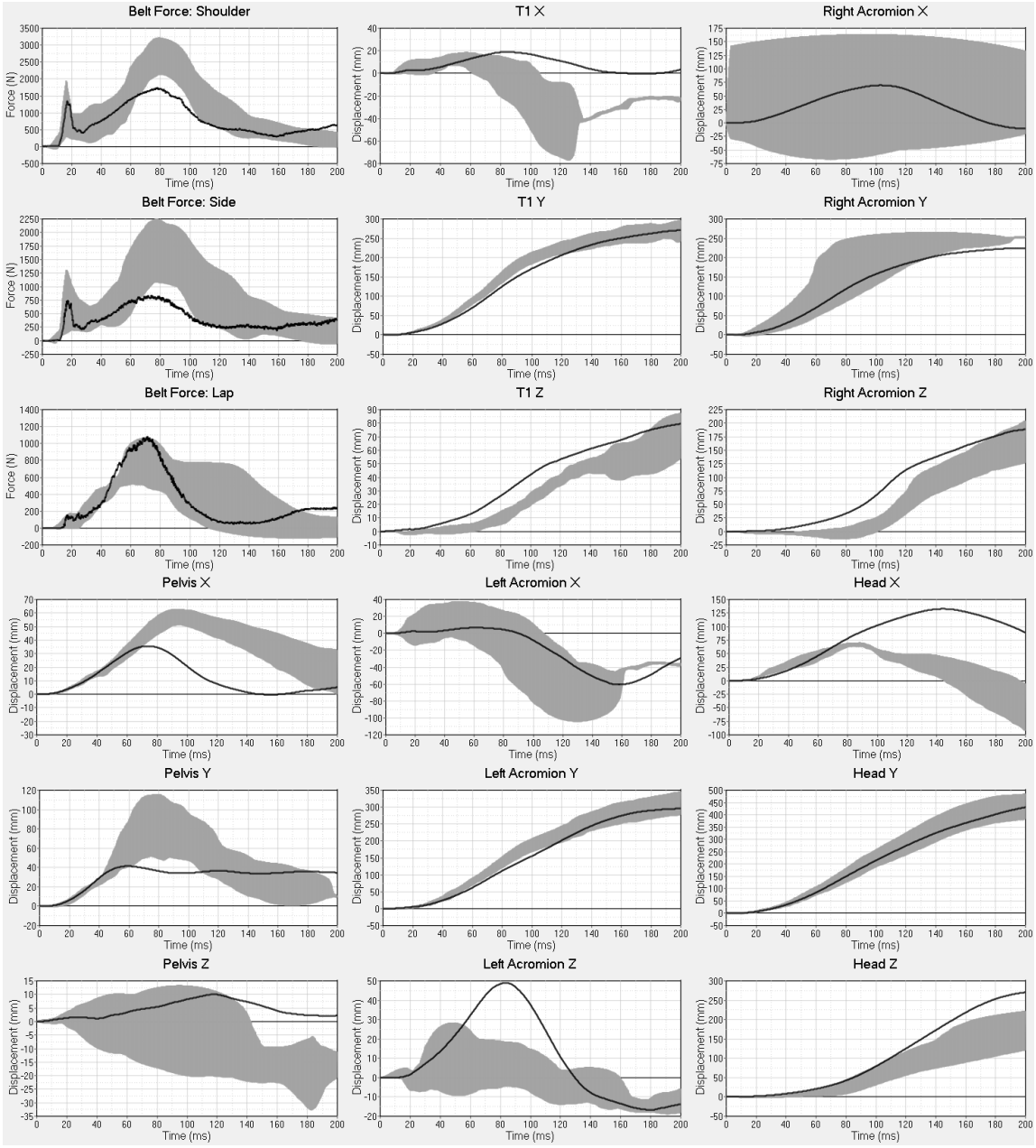

Fig. F 7. HBM responses and validation corridors from PMHS tests in [12], Configuration 4: Belt forces and kinematic signals.

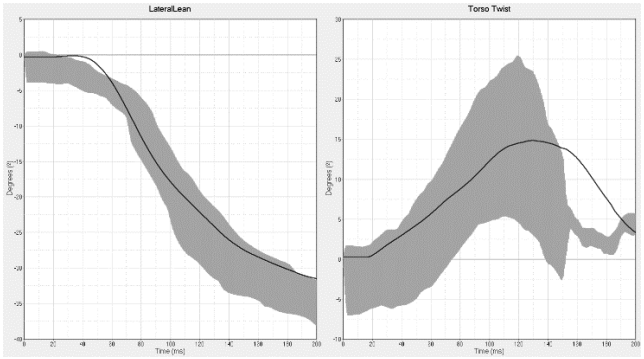

Fig. F 8. HBM responses and validation corridors from PMHS tests in [12], Configuration 4: Lateral lean and torso twist signals.

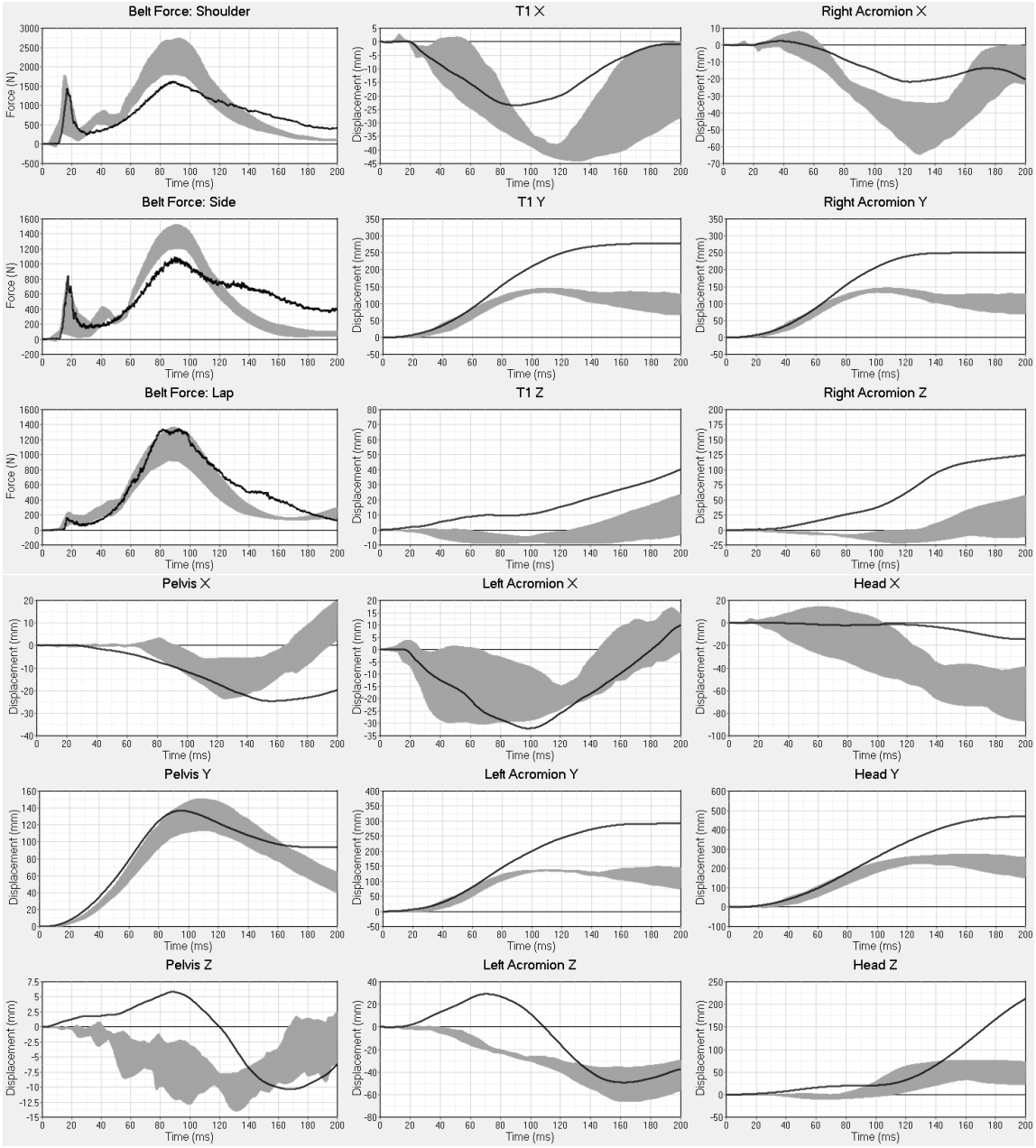

Fig. F 9. HBM responses and corridors from PMHS tests in [12], Configuration 5: Belt forces and kinematic signals

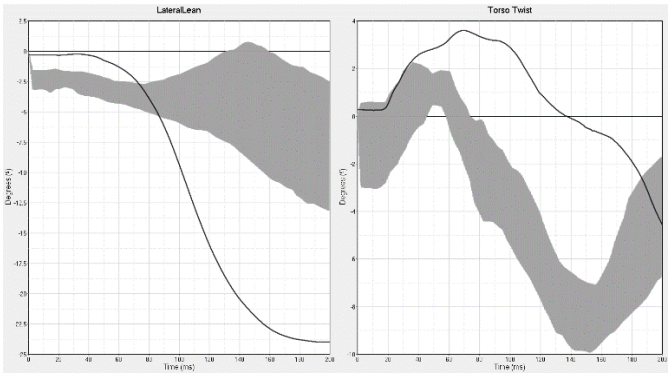

Fig. F 10. HBM responses and corridors from PMHS tests in [12], Configuration 5: Lateral lean and torso twist signals.

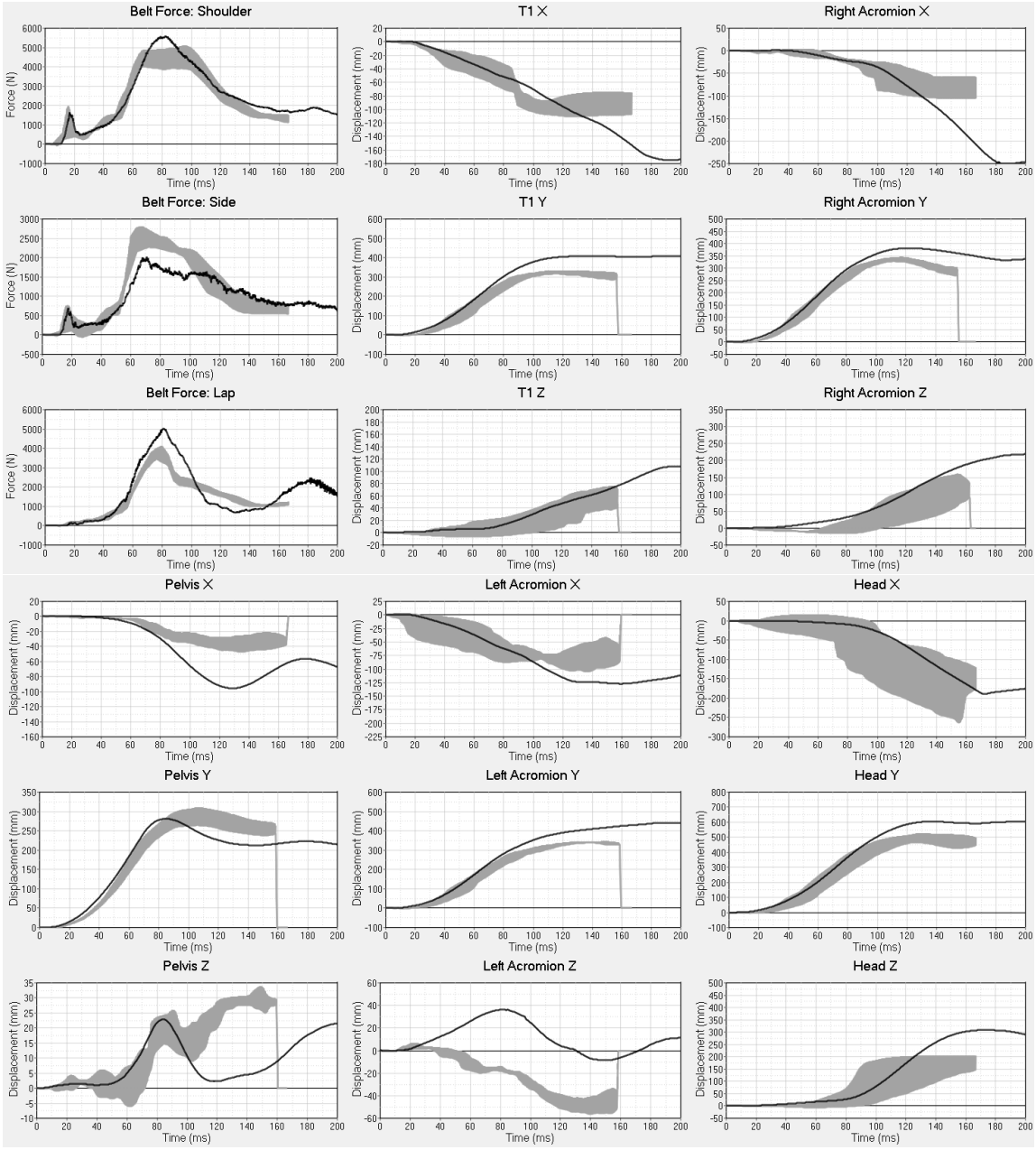

Fig. F 11. HBM responses and corridors from PMHS tests in [12], Configuration 6: Belt forces and kinematic signals.

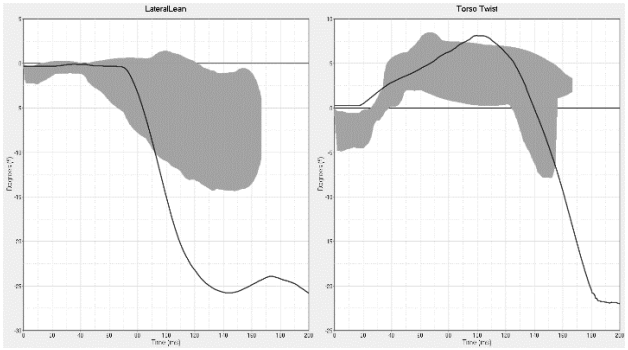

Fig. F 12. HBM responses and corridors from PMHS tests in [12], Configuration 6: Lateral lean and torso twist signals.

G. Simplified Far-Side Impact Set-Up; Result Table for Numerical Robustness Sub-Study

TABLE G I

PEAK BOUNDARY CONDITION VALUES, DISPLACEMENTS, AND CORA SCORES IN REPEATED SIMULATIONS OF THE SIMPLIFIED FAR-SIDE IMPACT VALIDATION SET-UP FOR [1,2,3,4,6]X32 CPU.

SD = STANDARD DEVIATION. CV = COEFFICIENT OF VARIATION, THE SD DIVIDED BY THE MEAN

	1x32 CPU	**2x32 CPU**	**3x32 CPU**	**4x32 CPU**	**6x32 CPU**	**Mean**	**SD**	**CV (%)**
Belt Force: Shoulder (N)	5564	5566	5569	5561	5555	5563	4.77	0.09
Belt Force: Side (N)	2157	2189	2174	2160	2173	2170.6	11.43	0.53
Belt Force: Lap (N)	4970	4946	4929	4933	4920	4939.6	17.35	0.35
T1 X (mm)	52.3	52.4	52.8	52.5	52.3	52.46	0.19	0.35
T1 Y (mm)	438.7	441.3	440.1	438.6	439.7	439.68	0.99	0.23
T1 Z (mm)	140.4	146.1	146.3	142	144.9	143.94	2.34	1.63
Right Acromion X (mm)	138.9	138.8	139	138.7	138.6	138.8	0.14	0.10
Right Acromion Y (mm)	364.7	366.7	365.3	364.7	365.3	365.34	0.73	0.20
Right Acromion Z (mm)	278.5	286.3	287	280.5	285.2	283.5	3.38	1.19
Pelvis X (mm)	54	54	54	54	54.1	54.02	0.04	0.07
Pelvis Y (mm)	172.6	173.3	171.8	173.6	172.3	172.72	0.66	0.38
Pelvis Z (mm)	16.7	16.5	16.7	16.7	16.6	16.64	0.08	0.48
Left Acromion X (mm)	28.7	28.8	28.8	28.6	28.9	28.76	0.10	0.35
Left Acromion Y (mm)	485.8	490.1	488.5	486.4	487.9	487.74	1.53	0.31
Left Acromion Z (mm)	64.8	65.2	65.3	65.3	65.4	65.2	0.21	0.32
Head X (mm)	170.2	170.3	170.8	170.3	171.6	170.64	0.52	0.31
Head Y (mm)	617.8	620.2	619.3	615.9	618.1	618.26	1.46	0.24
Head Z (mm)	286.7	289.7	291.3	288.7	290.6	289.4	1.61	0.56
LateralLean (degrees)	-37.8	-38.4	-38.4	-37.8	-38.2	-38.12	0.27	-0.71
Torso Twist (degrees)	27.7	28	27.9	27.4	27.8	27.76	0.21	0.74
CORA								
Boundary conditions	0.923	0.923	0.923	0.923	0.923	0.923	0.00	0.00
Kinematics	0.781	0.776	0.777	0.782	0.778	0.779	0.00	0.27
Overall	0.779	0.778	0.779	0.780	0.778	0.779	0.00	0.09

H. Vehicle-Based Far-Side Impact Validation Set-Up; CORA Scores

TABLE H I

CORA SCORES FOR EACH INDIVIDUAL COMPONENT FOR THE VEHICLE-BASED FAR-SIDE IMPACT VALIDATION SET-UP.

Configuration 7		Configuration 8	
Head X	0.23	*Head X*	0.46
Head Y	0.96	*Head Y*	0.92
Head Z	0.57	*Head Z*	0.35
Shoulder X	0.52	*Shoulder X*	0.65
Shoulder Y	0.84	*Shoulder Y*	0.97
Shoulder Z	0.83	*Shoulder Z*	0.40
Lap Belt Force	0.93	*Lap Belt Force*	0.89
Sternum X	0.74	*Sternum X*	0.60
Sternum Y	0.94	*Sternum Y*	0.97
Sternum Z	0.73	*Sternum Z*	0.51
Shldr Belt Force	0.91	*Shldr Belt Force*	0.96
Pre-Dring Belt force	0.93	*Pre-Dring Belt force*	0.91
Belt Payout	0.9	*Belt Payout*	0.42
Boundary Conditions	0.92	*Boundary Conditions*	0.79
Kinematics	0.71	*Kinematics*	0.65
Overall	0.77	*Overall*	0.69

I. Vehicle-Based Far-Side Impact Set-Up; Comparing Snapshots for SAFER HBM and PMHS from [18][19]

Fig. I 1. Test Configuration 7: SAFER HBM and the five PMHS tests from [18], at 110 ms.

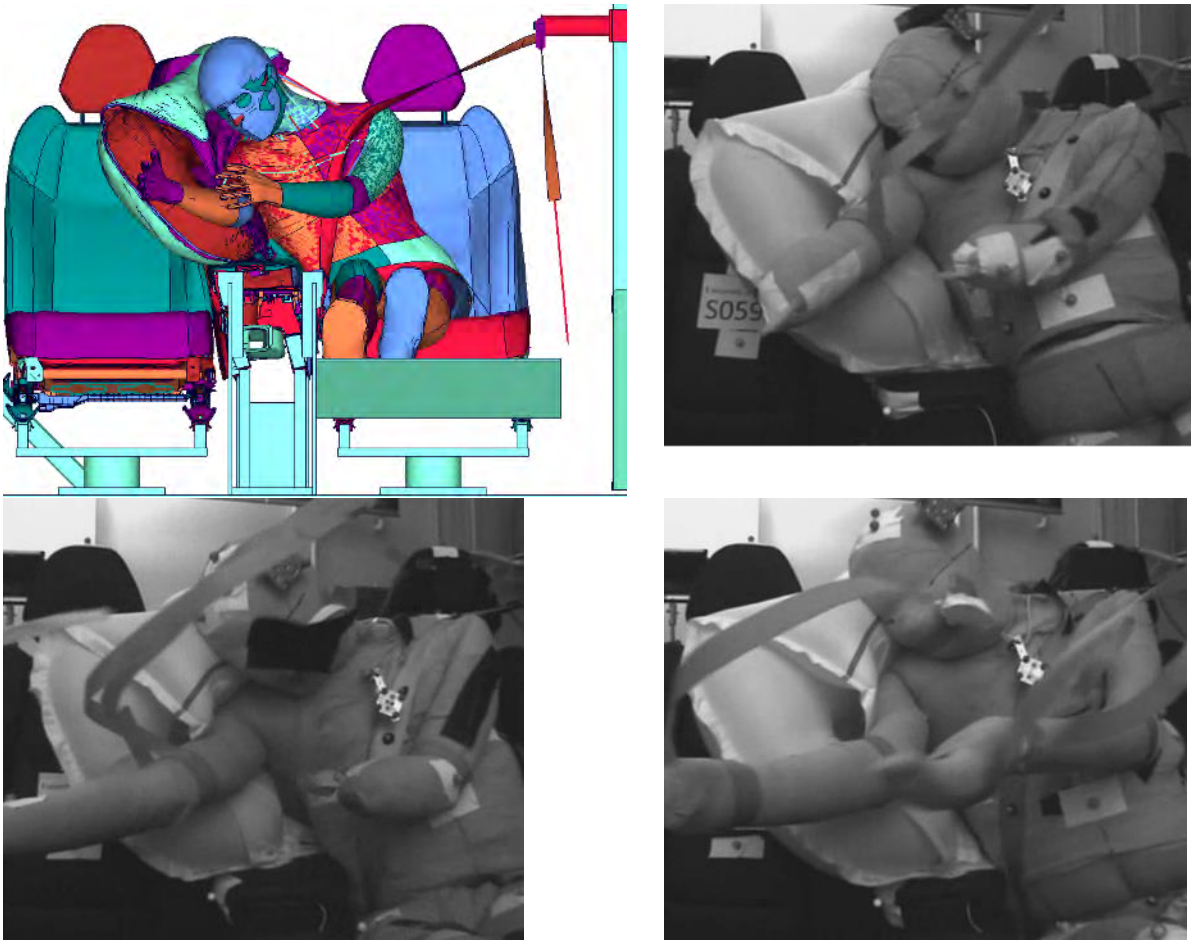

Fig. I 2. Test Configuration 8: SAFER HBM and the three PMHS tests in [19], at 100 ms.

J. Vehicle-Based Far-Side Impact Validation Set-Up; SAFER HBM Responses and PMHS Corridors created from Tests in [18] and [19]

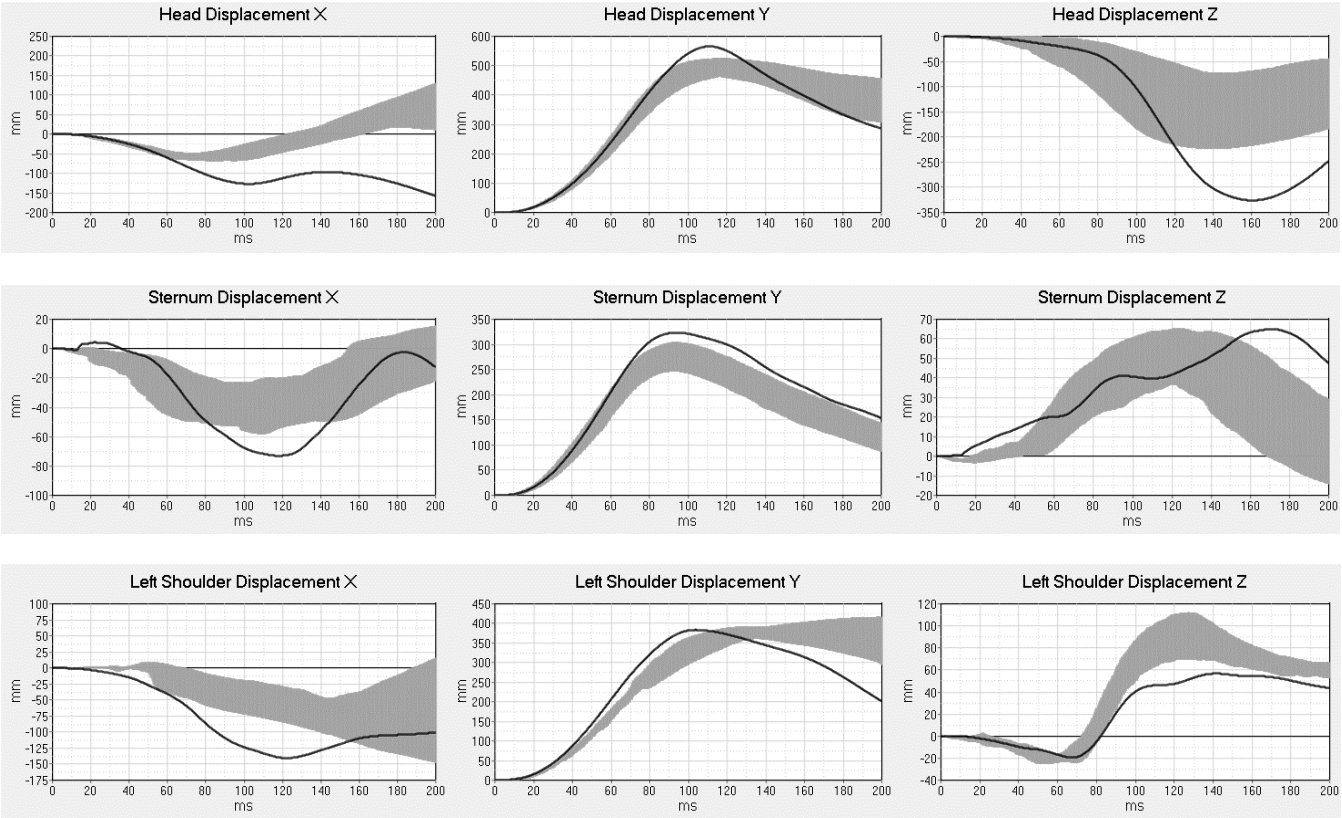

Fig. J 1. HBM responses and validation corridors created from PMHS tests [18] in Configuration 7 (without far-side airbag). Kinematic signals.

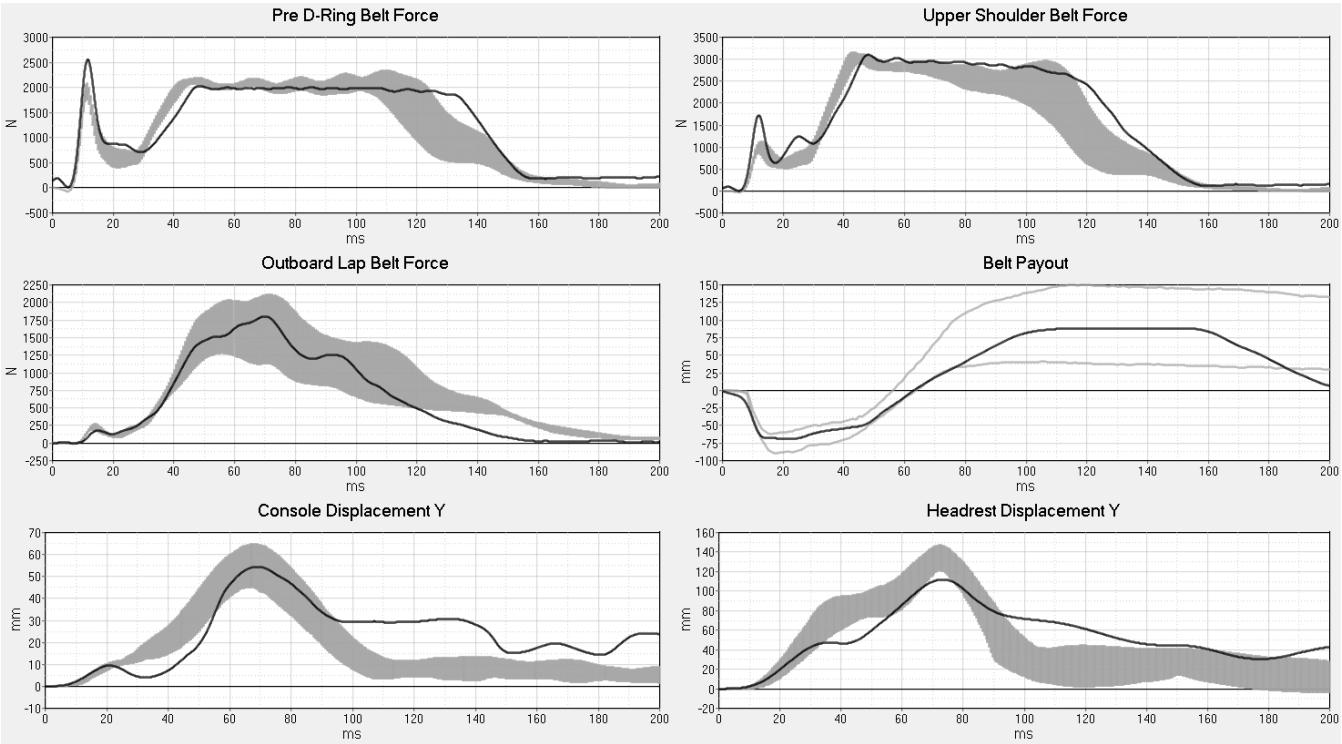

Fig. J 2. HBM response and PMHS validation created from PMHS tests [18] in Configuration 7 (without far-side airbag). Boundary condition signals.

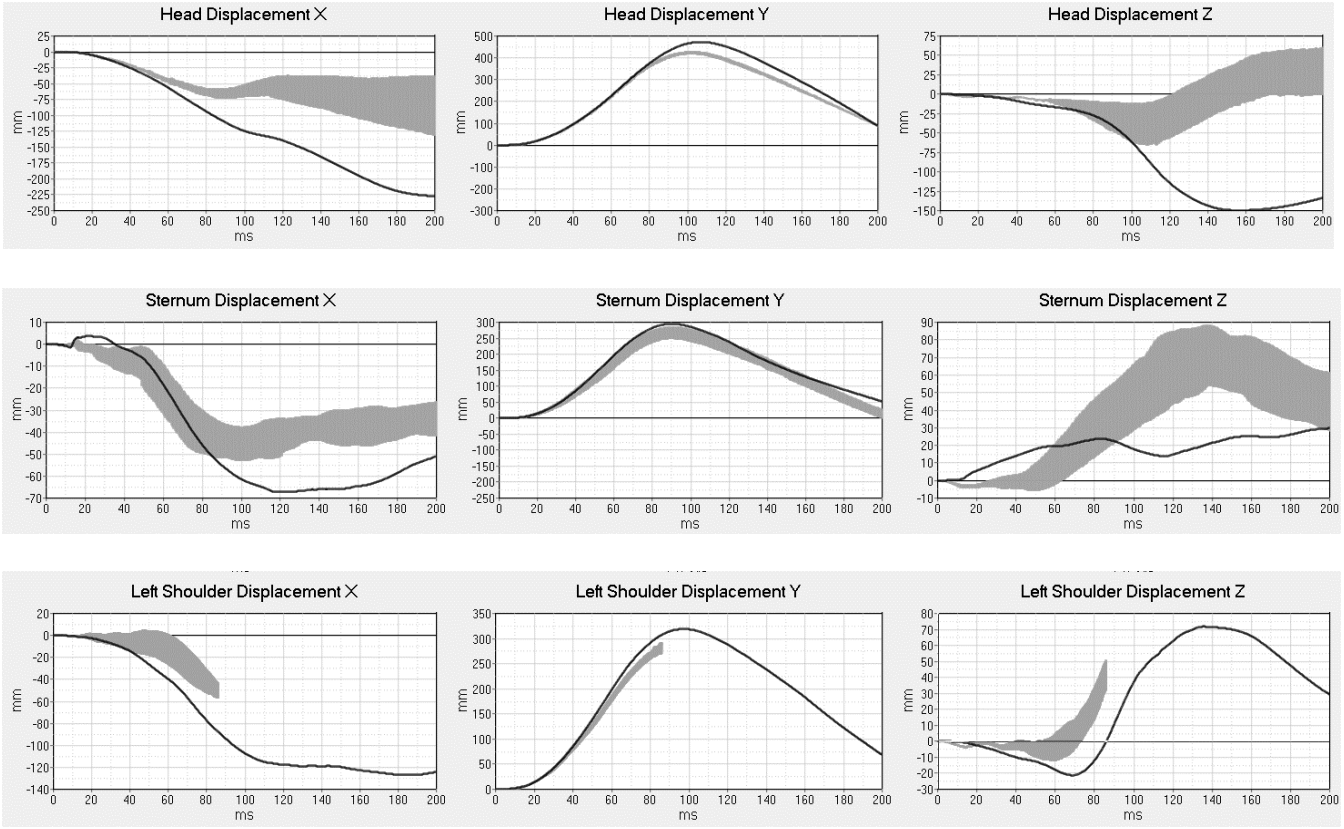

Fig. J 3. HBM response and PMHS validation corridors created from PMHS tests [19] in Configuration 8 (with far-side airbag). Kinematic signals.

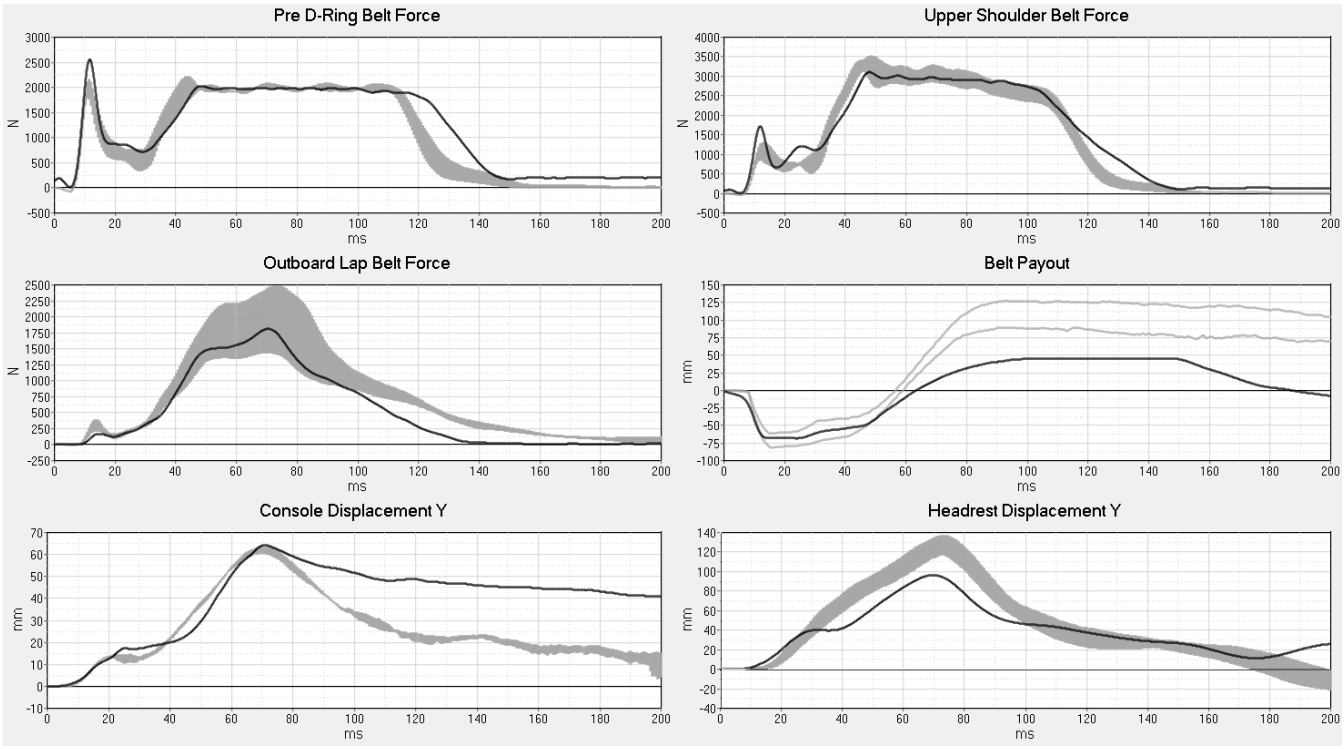

Fig. J 4. HBM response and PMHS validation corridors created from PMHS tests [19] in Configuration 8 (with far-side airbag). Boundary condition signals.

K. Mesh quality criteria

TABLE K I

MESH QUALITY CRITERIA USED FOR UPDATES OF THE SAFER HBM (SOFTWARE WITHIN BRACKETS DEFINES CRITERIA). SUPER SCRIPTS REFERS TO PUBLICATIONS OR OTHER SOURCES USED AS BASIS FOR CRITERIA LEVELS. THE 100% LIMIT IS MAINLY FOR OVERALL MODEL STABILITY AND SHOULD THUS BE FULFILLED FOR THE WHOLE MODEL. AREAS OF HIGH IMPORTANCE, WHERE TISSUE-BASED INJURY CRITERIA SHOULD BE USED, SHOULD ALSO FULFILL THE 95% TARGET.

	Aspect Ratio [-]	Skewness [deg]	Warpage [deg]	Hexa Angle [deg]	Tetra Angle [deg]	Jacobian [-]
Solid Elements	(Patran)	(Patran)	(Patran)	(Abaqus)	(Abaqus)	(ANSA)
95 % Target	$<3^{a-c}$	$<45^{b}$	$<10^{c}$	$30<\phi<140^{c}$	$30<\phi<120^{b}$	$>0.7^{a,c}$
100 % Limit	$<10^{a,c}$	$<60^{b}$	$<20^{b}$	$20<\phi<160^{a}$	$20^{c}<\phi<150^{a}$	$>0.3^{c}$

	Aspect Ratio [-]	Skewness [deg]	Warpage [deg]	Quad Angle [deg]	Tria Angle [deg]	Jacobian [-]
Shell elements	(Patran)	(Patran)	(Patran)	(IDEAS)	(IDEAS)	(ANSA)
95 % Target	$<3^{a-c}$	$<30^{c}$	$<7^{c}$	$45<\phi<135^{b,c}$		$>0.7^{a,c}$
100 % Limit	$<10^{b}$	$<60^{b}$	$<20^{b}$	$20<\phi<160^{c}$	$30<\phi<120^{b,c}$	$>0.3^{c}$

[a] Burkhart, T. A., Andrews, D. M., & Dunning, C. E. (2013). Finite element modeling mesh quality, energy balance and validation methods: a review with recommendations associated with the modeling of bone tissue. *Journal of biomechanics, 46*(9), 1477-1488

[b] Yang, K.-H. (2017). *Basic finite element method as applied to injury biomechanics*: Academic Press.

[c] Industry requirements